



Norwegian University of
Science and Technology

Nonlinear control of Tethered Airfoils

Path-following control of Tethered Airfoils

Håvard Knappskog

Master of Science in Engineering Cybernetics

Submission date: June 2011

Supervisor: Kristin Ytterstad Pettersen, ITK

Co-supervisor: Jan Hystad, Kraftkite

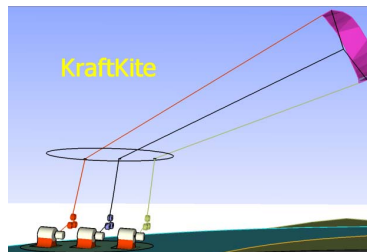
Norwegian University of Science and Technology
Department of Engineering Cybernetics



MASTEROPPGAVE

Kandidatens navn: **Håvard Knappskog**
Fag: **Teknisk kybernetikk**
Oppgavens tittel (norsk): **Ulineær kontroll av forankrede vingeprofilier**
Oppgavens tittel (engelsk): **Nonlinear control of tethered airfoils**
Oppgavens tekst:

The International Energy Agency (IEA) estimates the need for installing more than 47 GW new wind capacity at an estimated cost of 500 billion NOK each year until 2050 if we are to meet the renewable targets set to tackle global warming. Innovasjon Norge is supporting KraftKite to investigate the possibilities of using kites to produce electricity in a radical new approach. Kites will enable a solution that replaces some of the more expensive components of today's wind mills, and thus drastically reduce costs. Kites have just been introduced for propulsion of ships, but are novel instruments in electricity production. One of the key challenges will be automated control of kites given the relatively large variations in the wind conditions. For a system to be commercially successful the flight of the kites must have very high reliability. The task at hand will be modeling of the kites, consideration of needed sensor technology and design of a control strategy to maximize the power output.



Preliminary set of tasks:

1. Develop a mathematical model for a tethered airfoil.
2. Adjust the model for a standard surf kite, to facilitate proto-testing.
3. Develop a control law for path following or way-point tracking, and verify the model behavior by simulations.
4. Investigate the stability properties of the closed loop system.

Oppgaven gitt: 11.01.2011

Besvarelsen leveres: 07.06.2011

Utført ved Institutt for teknisk kybernetikk

Medveileder:

PhD Jan Hystad, KraftKite

Trondheim, den 11.01.2011

Kristin Y. Pettersen

Faglærer

Abstract

This master thesis contains modeling, analysis and control design for a tethered airfoil. A path-following controller has been developed and proven locally asymptotically stable. The guidance law is general, and applicable to other path-following systems. The closed loop system is demonstrated in simulations, where a certain level of robustness is concluded.

Preface

This master thesis is conducted during spring 2011 at the Department of Engineering Cybernetics under the Norwegian University of Science and Technology.

Investigating automated control of kites was initially motivated by my co-supervisor Jan Hystad and his co-workers from Kraftkite. The effort on solving this problem has led to an increasing interest in the field for both me and my fellow students.

I would like to thank my main supervisor Professor Kristin Y. Pettersen for valuable help and throughout this semester. I would also like to thank my co-supervisor Jan Hystad for inspiration and practical instruction of flying kites.

Also, I would like to thank my class and lunch-mates Trygve Utstumo, Ola Hjukse and Erik Hannisdal for keeping up the spirit, and my girlfriend Veronique Aalmo for invaluable inspiration throughout the every day.

Håvard Knappskog
Trondheim, June 6, 2011

Contents

1	Introduction	1
1.1	Motivation	1
1.2	Outline	1
1.3	Tethered airfoils	2
2	Modeling	5
2.1	Introduction	5
2.2	Kinematic model	5
2.3	Coordinate frames and transformations	10
2.4	Aerodynamic forces	16
2.5	Kite model in state space	20
3	Control design	23
3.1	Introduction	23
3.2	Path-frame	24
3.3	The movement-frame	28
3.4	Path error in cartesian coordinates	30
3.5	Path following system	32
3.5.1	Guidance law	32
3.5.2	Stability analysis of the nominal system	32
3.6	Controller dynamics	38

4	Simulation	43
4.1	Introduction	43
4.2	Parametric curve in spherical coordinates	43
4.3	Simulation with ideal conditions	47
4.4	Simulation with wind turbulence	53
5	Conclusion	59
6	Further work	61

List of Figures

1.1	Area of operation for a tethered airfoil.	2
2.1	Spherical coordinates	7
2.2	The local frame and the body frame.	9
2.3	The body frame and the wind vector	13
2.4	Overview of parameters and dimensions of the kite	17
2.5	Aerodynamic coefficients and glide ratio.	18
3.1	Path frame	25
3.2	Visualization of the set Ω_c	38
4.1	Parametric curve γ in $\theta\phi$ -plane.	45
4.2	3D trajectory, path-following system	48
4.3	XZ-trajectory for the path-following system.	49
4.4	XY-trajectory for the path-following system.	50
4.5	XYZ path error.	50
4.6	Yawing angles, β_b and $\beta_{b,d}$	51
4.7	Control input from simulation.	51
4.8	Control state δ_l	52
4.9	Angle of attack, α_{aoa}	53
4.10	3D trajectory, path-following system	54
4.11	XZ-trajectory for the path-following system.	55
4.12	XY-trajectory for the path-following system.	55
4.13	Control input from simulation.	56

4.14	Control state δ_l	57
4.15	Angle of attack, α_{aoa}	57
4.16	Wind speed and direction in the xy-plane.	58

Chapter 1

Introduction

1.1 Motivation

The most obvious applications for tethered airfoils, often referred to as kites, are propulsion, and power generation. Using kites for propulsion is a proven concept, seen in the kitesurfing sport. The world speed record for sailing, was performed using kites for propulsion [2]. For power generation, tethered airfoils have numerous benefits compared to traditional wind-mills, as pointed out by [1],[6]. One of the key challenges yet to be solved for use in industrial applications, either for propulsion or power generation, is a reliable control system for automated operation.

1.2 Outline

A short description of the chapters contained in this thesis is given:

2 Modelling - A kinematic model is developed, including aerodynamic forces and reference frames.

3 Control Design - With the kinematic model as a starting point, a control system for path following is proposed.

4 Simulation - The closed loop system from the two previous chapters is simulated and presented in this chapter.

5 Conclusion - Conclusions are drawn based on the results in this thesis.

6 Further Work - Suggested topics and issues for further work are presented in this chapter.

1.3 Tethered airfoils

The terminology *kite* and *tethered airfoil* are used interchangeably, although the latter is more common in literature. Figure 1.1 illustrates the concept of a tethered airfoil. The airfoil is fixed to the ground, or some object on the ground by a cable with length r . The movement is restricted to the spherical surface given by the cable length. The blue lines in Figure 1.1 indicate

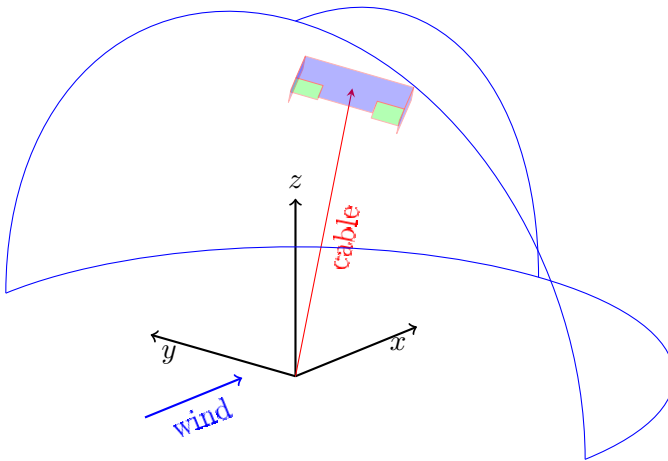


Figure 1.1: Area of operation for a tethered airfoil.

the reachable area, which is limited by the wind direction, and the ground in the xy -plane. The airfoil may neither fly past the attachment point in

upwind direction, nor fly below ground. This means $x, z > 0$.

There are different ways to optimise the trajectory for a tethered airfoil. When the trajectory is optimized with respect to the direction and the amplitude of the force exerted on the cable, the actual position is of less importance. This force is what generates either propulsion, or power. The maximum force is achieved when flying with high velocity, in the downwind (x-direction) sector. The least amount of force is achieved by hovering stationary close to the yz-plane.

Chapter 2

Modeling

2.1 Introduction

Substantial effort has been made prior to this research on modelling tethered airfoils. In particular, the model presented in [6] is highly detailed. The purpose of this model, is the use of (nonlinear)model-predictive control (MPC). Such a technique would only benefit from a detailed model [12]. The control strategy attempted in this research, on the other hand, would not necessarily benefit from a certain level of detail. The techniques used in this thesis is reliant on analytical calculations to be performed on the model. Therefore, the focus of the modelling in this chapter is to keep it as simple as possible, without compromising the details needed to resemble the behaviour of a real tethered airfoil.

2.2 Kinematic model

The following kinematic model is a recognised model for kinematics in spherical coordinates. It has been presented in [8], also derived in detail in the pre-project [11] to this thesis. The key elements are repeated for full overview. The Euler-Lagrange equation is used to derive the model, with

$\mathbf{q} = (\theta \ \phi \ r)^T$ being the spherical coordinates.

$$\frac{d}{dt} \left(\frac{\partial L}{\partial \dot{\mathbf{q}}_i} \right) - \frac{\partial L}{\partial \mathbf{q}_i} = \tau_i \quad (2.1)$$

$L(\mathbf{q}, \dot{\mathbf{q}}, t)$ is given,

$$L(\mathbf{q}, \dot{\mathbf{q}}, t) = T(\mathbf{q}, \dot{\mathbf{q}}, t) - U(\mathbf{q}) \quad (2.2)$$

where T is the kinetic-, and U the potential energy.

$$T_{kin} = \frac{1}{2} \bar{m} |\dot{\mathbf{p}}|^2 = \frac{\bar{m}}{2} \left(\dot{r}^2 + r^2 \sin^2(\theta) \dot{\phi}^2 + r^2 \dot{\theta}^2 \right) \quad (2.3)$$

$$U = mgh = mgr \cos(\theta) \quad (2.4)$$

\bar{m} is the effective kinetic mass, given that the mass of the cable is distributed along the distance r . If the cable is light compared to the mass of the kite m , we assume $\bar{m} = m$, and the result is given:

$$\boxed{\ddot{\mathbf{q}} = S^{-1} \frac{F^l}{m} - \mathbf{a}} \quad (2.5)$$

Where S is a scaling matrix,

$$S = \begin{pmatrix} r & 0 & 0 \\ 0 & r \sin \theta & 0 \\ 0 & 0 & 1 \end{pmatrix} \quad (2.6)$$

and \mathbf{a} is the pseudo force:

$$\mathbf{a} = \begin{pmatrix} 2 \frac{\dot{r}}{r} \dot{\theta} - \sin \theta \cos \theta \dot{\phi}^2 \\ 2 \frac{\dot{r}}{r} \dot{\phi} + 2 \frac{\cos \theta}{\sin \theta} \dot{\theta} \dot{\phi} \\ -r \sin \theta \dot{\phi}^2 - r \dot{\theta}^2 \end{pmatrix} \quad (2.7)$$

F^l is the sum of forces given in the local system:

$$F^l = F_g^l + F_{aer}^l + F_c^l \quad (2.8)$$

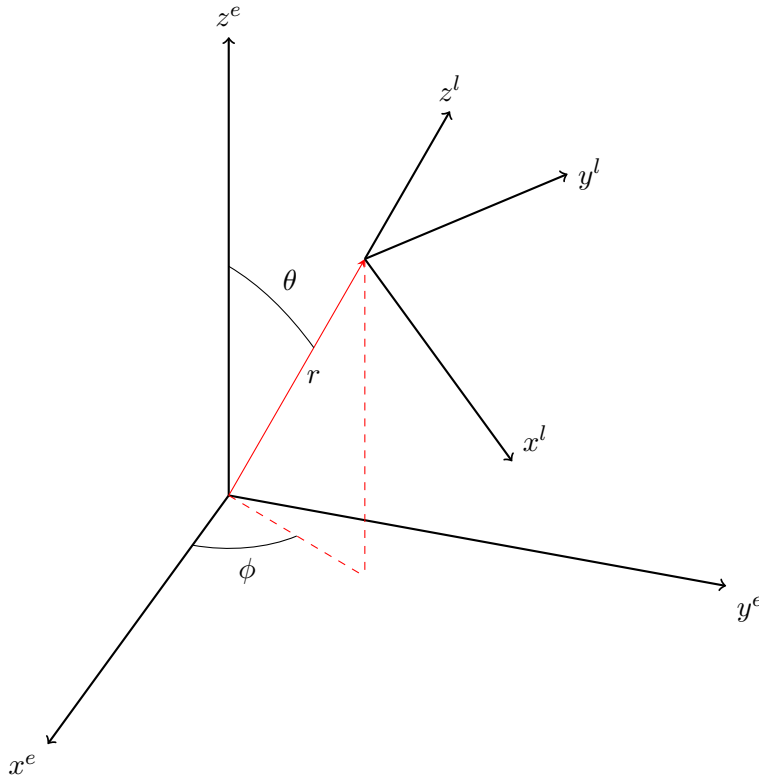


Figure 2.1: The earth and local coordinate systems. The spherical coordinates $\mathbf{q} = (\theta, \phi, r)^T$ are indicated in the figure.

Where F_g^l is the gravity:

$$F_g^l = m \begin{pmatrix} g \sin \theta \\ 0 \\ -g \cos \theta \end{pmatrix} \quad (2.9)$$

ans F_{aer} and F_c is the aerodynamic and the cable force. For a more intuitive understanding of the above equation, it is written in scalar form:

$$\ddot{\theta} = \frac{F_\theta}{mr} - a_\theta \quad (2.10)$$

$$\ddot{\phi} = \frac{F_\phi}{mr \sin \theta} - a_\phi \quad (2.11)$$

$$\ddot{r} = \frac{F_r}{m} - a_r \quad (2.12)$$

This is a general kinematic model of a body in spherical coordinates, the way it is presented in recognized literature, [1][6][8][9].

The model is adapted for the specific case where r is a constant parameter of the system. In this case, the cable force F_c^l will cancel out any other force in the e_r -direction such that $F_3^l = 0$:

$$F_c^l = - \left(F_g^l + F_{aer}^l \right)_3 \quad (2.13)$$

Furthermore, two additional states are added, the yaw β_b of the kite body around the cable and the flaps angle δ_l . With these modifications, the kite model is given:

$$\begin{pmatrix} \ddot{\theta} \\ \ddot{\phi} \\ \dot{\beta}_b \\ \dot{\delta}_l \end{pmatrix} = \begin{pmatrix} \left(S^{-1} \frac{F^l}{m} - \mathbf{a} \right)_1 \\ \left(S^{-1} \frac{F^l}{m} - \mathbf{a} \right)_2 \\ \frac{M_k}{I_k} \\ b_u u \end{pmatrix} \quad (2.14)$$

where M_k is the moment and I_k is the moment of inertia in the yaw-axis. u is the control input, and b_u is the actuator gain.

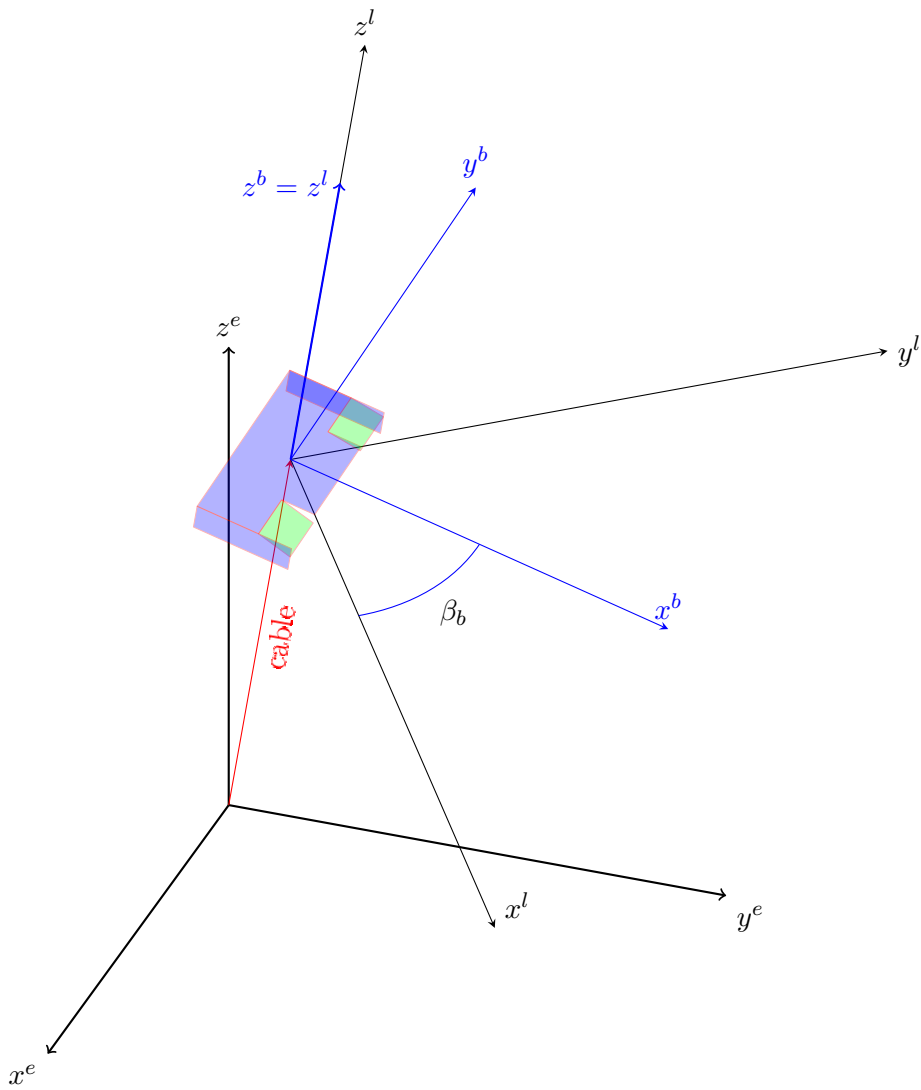


Figure 2.2: This figure shows the local frame and the body frame rotated around the z -axis by the angle β_b .

2.3 Coordinate frames and transformations

In this section, the reference frames and the transformations between them will be explained. The following right-handed orthogonal reference frames are defined, with corresponding unit vectors in the x-, y- and z-direction:

- Earth frame \mathcal{F}_e , unit vectors: \vec{e}_x , \vec{e}_y and \vec{e}_z .
- Local frame \mathcal{F}_l , unit vectors: \vec{e}_θ , \vec{e}_ϕ and \vec{e}_r .
- Body frame \mathcal{F}_b , unit vectors: \vec{e}_i , \vec{e}_j and \vec{e}_k .
- Wind frame \mathcal{F}_w , unit vectors: \vec{e}_w , \vec{e}_t and \vec{e}_n .

Any additional orthogonal unitvectors will be given $\vec{e}_{1,p}$, $\vec{e}_{2,p}$ and $\vec{e}_{3,p}$ where p indicates the corresponding frame, in this case the path-frame discussed in Chapter 3. A rotation between any of the above frames is performed with a combination of the following rotation matrices:

$$R_x(\theta) = \begin{pmatrix} 1 & 0 & 0 \\ 0 & \cos \theta & \sin \theta \\ 0 & -\sin \theta & \cos \theta \end{pmatrix} \quad (2.15)$$

$$R_y(\theta) = \begin{pmatrix} \cos \theta & 0 & -\sin \theta \\ 0 & 1 & 0 \\ \sin \theta & 0 & \cos \theta \end{pmatrix} \quad (2.16)$$

$$R_z(\theta) = \begin{pmatrix} \cos \theta & \sin \theta & 0 \\ -\sin \theta & \cos \theta & 0 \\ 0 & 0 & 1 \end{pmatrix} \quad (2.17)$$

In equation (2.5), the forces are given in the local frame at the position of the kite. The transformation between the earth frame and the local frame is defined:

$$\mathbf{v}^l = R_e^l \mathbf{v}^e \quad (2.18)$$

Where \mathbf{v}^e is any vector given in the earth frame, \mathbf{v}^l is given in the local frame, R_e^l is the rotation matrix between the two frames. R_e^l consists of two rotations, first one rotation around the z-axis, then around the y axis:

$$\begin{aligned} R_e^l &= R_y(\theta)R_z(\phi) \\ &= \begin{pmatrix} \cos(\theta)\cos(\phi) & \cos(\theta)\sin(\phi) & -\sin(\theta) \\ -\sin(\phi) & \cos(\phi) & 0 \\ \sin(\theta)\cos(\phi) & \sin(\theta)\sin(\phi) & \cos(\theta) \end{pmatrix} \end{aligned} \quad (2.19)$$

Recall equations (2.15) - (2.17). Figure 2.1 shows the spherical coordinates and the relation between the two frames.

While the kite is manoeuvred in space, it may rotate around its yaw-axis(z-axis of the local-frame). This rotation is the transformation between the local-frame and the body-frame:

$$R_l^b = R_z(\beta_b) \quad (2.20)$$

$$R_l^b = \begin{pmatrix} \cos \beta_b & \sin \beta_b & 0 \\ -\sin \beta_b & \cos \beta_b & 0 \\ 0 & 0 & 1 \end{pmatrix} \quad (2.21)$$

This rotation is illustrated in Figure 2.2. Note that the xy-plane is the same for the two frames.

The aerodynamic forces are defined in the wind-frame. It is intuitive that the sideforce should be in the xy-plane of the body frame. This determines the sequence of rotations between the body-frame and the wind-frame. There are two rotations, first around the z-axis, second, around the

y-axis:

$$\begin{aligned}
 R_b^w &= R_y(\alpha_w)R_z(\beta_s) \\
 &= \begin{pmatrix} \cos \alpha_w & 0 & -\sin \alpha_w \\ 0 & 1 & 0 \\ \sin \alpha_w & 0 & \cos \alpha_w \end{pmatrix} \begin{pmatrix} \cos \beta_s & \sin \beta_s & 0 \\ -\sin \beta_s & \cos \beta_s & 0 \\ 0 & 0 & 1 \end{pmatrix} \\
 &= \begin{pmatrix} \cos \alpha_w \cos \beta_s & \cos \alpha_w \sin \beta_s & -\sin \alpha_w \\ -\sin \beta_s & \cos \beta_s & 0 \\ \sin \alpha_w \cos \beta_s & \sin \alpha_w \sin \beta_s & \cos \alpha_w \end{pmatrix} \quad (2.22)
 \end{aligned}$$

This is illustrated in Figure 2.3. The yaw-angle β_b is a known state of the system, while the yaw-angle β_s and the pitch-angle α_w is a product of the states, and the wind vector w . The angles α_w and β_s may be calculated from the wind vector.

The relative, or the effective wind vector given in the local frame is defined as:

$$\mathbf{w}_e^l = \mathbf{w}^l - \dot{\mathbf{p}} = R_e^l \mathbf{w}^e - \dot{\mathbf{p}} \quad (2.23)$$

With the wind set to be in the x-direction of the earth frame, and $\dot{r} = 0$, the relative wind is calculated:

$$\mathbf{w}_e^l = R_e^l \mathbf{w}^e - \dot{\mathbf{p}}^l \quad (2.24)$$

$$= \begin{pmatrix} c\theta c\phi & c\theta s\phi & -s\theta \\ -s\phi & c\phi & 0 \\ s\theta c\phi & s\theta s\phi & c\theta \end{pmatrix} \begin{pmatrix} w \\ 0 \\ 0 \end{pmatrix} - \begin{pmatrix} r\dot{\theta} \\ rs\theta\dot{\phi} \\ 0 \end{pmatrix} \quad (2.25)$$

$$= \begin{pmatrix} wc\theta c\phi - r\dot{\theta} \\ -ws\phi - rs\theta\dot{\phi} \\ ws\theta c\phi \end{pmatrix} = \begin{pmatrix} w_{e1} \\ w_{e2} \\ w_{e3} \end{pmatrix} \quad (2.26)$$

The unitvectors of the wind-frame are \vec{e}_w , \vec{e}_t and \vec{e}_n . \vec{e}_w is in the direction of the relative wind \vec{w}_e . \vec{e}_t is the transversal axis of the wind-frame, which is perpendicular to both \vec{w}_e and \vec{e}_r . $\vec{e}_n = \vec{e}_w \times \vec{e}_t$ completes the wind-frame.

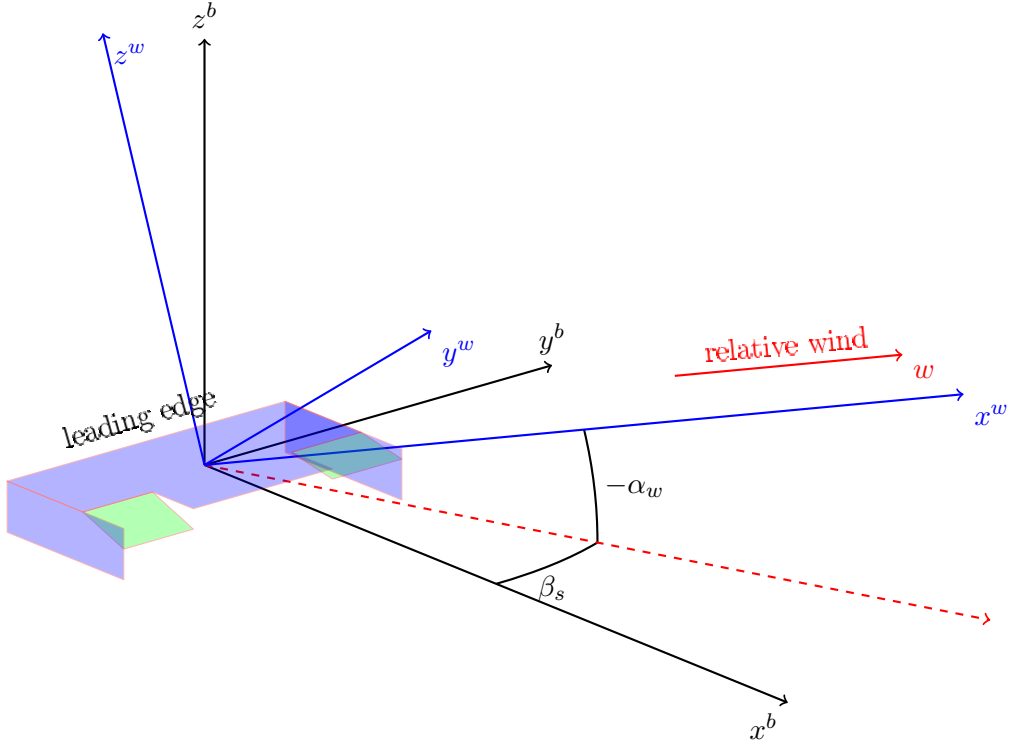


Figure 2.3: The relative wind vector is shown in the body frame.

The given properties lead to the following definition of the wind-frame:

$$\begin{aligned}
 \mathbf{e}_w^l &= \frac{\mathbf{w}_e}{|\mathbf{w}_e|} = \frac{1}{\sqrt{w_{e1}^2 + w_{e2}^2 + w_{e3}^2}} \begin{pmatrix} w_{e1} \\ w_{e2} \\ w_{e3} \end{pmatrix} \\
 &= \frac{1}{\sqrt{(w c \theta c \phi - r \dot{\theta})^2 + (w s \phi + r s \theta \dot{\phi})^2 + (w s \theta c \phi)^2}} \begin{pmatrix} w c \theta c \phi - r \dot{\theta} \\ -w s \phi - r s \theta \dot{\phi} \\ w s \theta c \phi \end{pmatrix}
 \end{aligned} \tag{2.27}$$

$$\begin{aligned} \mathbf{e}_t^l &= \frac{-w_e \times e_r}{|w_e \times e_r|} = \frac{1}{\sqrt{w_{e1}^2 + w_{e2}^2}} \begin{pmatrix} -w_{e2} \\ w_{e1} \\ 0 \end{pmatrix} \\ &= \frac{1}{\sqrt{(w\dot{c}\theta c\phi - r\dot{\theta})^2 + (ws\phi + rs\theta\dot{\phi})^2}} \begin{pmatrix} ws\phi + rs\theta\dot{\phi} \\ w\dot{c}\theta c\phi - r\dot{\theta} \\ 0 \end{pmatrix} \end{aligned} \quad (2.28)$$

$$\begin{aligned} \mathbf{e}_n^l &= \frac{-w_e \times (w_e \times e_r)}{|w_e \times (w_e \times e_r)|} = \frac{w_e \times e_t^*}{|w_e \times e_t^*|} = \frac{1}{\sqrt{w_{e1}^2 + w_{e2}^2 + w_{e3}^2} \sqrt{w_{e1}^2 + w_{e2}^2}} \begin{pmatrix} -w_{e1}w_{e3} \\ -w_{e2}w_{e3} \\ w_{e1}^2 + w_{e2}^2 \end{pmatrix} \\ &= \frac{1}{\sqrt{(w\dot{c}\theta c\phi - r\dot{\theta})^2 + (ws\phi + rs\theta\dot{\phi})^2 + (ws\theta c\phi)^2} \sqrt{(w\dot{c}\theta c\phi - r\dot{\theta})^2 + (ws\phi + rs\theta\dot{\phi})^2}} \\ &\quad \begin{pmatrix} -(w\dot{c}\theta c\phi - r\dot{\theta})(ws\theta c\phi) \\ (-ws\phi - rs\theta\dot{\phi})(ws\theta c\phi) \\ (w\dot{c}\theta c\phi - r\dot{\theta})^2 + (-ws\phi - rs\theta\dot{\phi})^2 \end{pmatrix} \end{aligned} \quad (2.29)$$

The above equations define the R_w^l :

$$R_w^l = (\mathbf{e}_w^l \quad \mathbf{e}_t^l \quad \mathbf{e}_n^l) \quad (2.30)$$

Furthermore, the above rotation is related to the body-frame:

$$R_w^b = R_b^{wT} = R_l^b R_w^l \quad (2.31)$$

From this definition of R_b^w given in equation (2.31), the angles α_w and β_s may be calculated. The result is expanded for further calculations.

$$(\mathbf{e}_w^b \quad \mathbf{e}_t^b \quad \mathbf{e}_n^b) = \begin{pmatrix} \cos \alpha_w \cos \beta_s & \boxed{-\sin \beta_s} & \sin \alpha_w \cos \beta_s \\ \cos \alpha_w \sin \beta_s & \cos \beta_s & \sin \alpha_w \sin \beta_s \\ \boxed{-\sin \alpha_w} & 0 & \cos \alpha_w \end{pmatrix} = R_l^b R_w^l \quad (2.32)$$

Note the two elements of the above matrix indicated by a box. These allow for the angles α_w and β_s to be extracted:

$$\alpha_w = -\arcsin(e_{w3}^b) \quad (2.33)$$

$$\beta_s = -\arcsin(e_{t1}^b) \quad (2.34)$$

Under the assumption that $|\alpha_w|, |\beta_s| < 90^\circ$, no quadrant corrections are needed in the arcsin calculation. This assumption is valid as long as the kite is not flying backwards, which would be a faulty behaviour. α_w and β_s needs to be expressed as functions of the states of the system for further analysis.

$$\begin{aligned} \mathbf{e}_w^b &= R_l^b \mathbf{e}_w^l \\ &= \frac{1}{\sqrt{\dots}} \begin{pmatrix} c\beta_b & s\beta_b & 0 \\ -s\beta_b & c\beta_b & 0 \\ 0 & 0 & 1 \end{pmatrix} \begin{pmatrix} wc\theta c\dot{\phi} - r\dot{\theta} \\ -ws\phi - rs\theta\dot{\phi} \\ ws\theta c\phi \end{pmatrix} \end{aligned} \quad (2.35)$$

$$e_{w3}^b = \frac{ws\theta c\phi}{\sqrt{(wc\theta c\phi - r\dot{\theta})^2 + (ws\phi + rs\theta\dot{\phi})^2 + (ws\theta c\phi)^2}} \quad (2.36)$$

$$\begin{aligned} \mathbf{e}_t^b &= R_l^b \mathbf{e}_t^l \\ &= \frac{1}{\sqrt{\dots}} \begin{pmatrix} c\beta_b & s\beta_b & 0 \\ -s\beta_b & c\beta_b & 0 \\ 0 & 0 & 1 \end{pmatrix} \begin{pmatrix} ws\phi + rs\theta\dot{\phi} \\ wc\theta c\phi - r\dot{\theta} \\ 0 \end{pmatrix} \end{aligned} \quad (2.37)$$

$$e_{t1}^b = \frac{c\beta_b(ws\phi + rs\theta\dot{\phi}) + s\beta_b(wc\theta c\phi - r\dot{\theta})}{\sqrt{(wc\theta c\phi - r\dot{\theta})^2 + (ws\phi + rs\theta\dot{\phi})^2}} \quad (2.38)$$

Which leads to the final expression for α_w and β_s :

$$\alpha_w = -\arcsin\left(\frac{ws\theta c\phi}{\sqrt{(wc\theta c\phi - r\dot{\theta})^2 + (ws\phi + rs\theta\dot{\phi})^2 + (ws\theta c\phi)^2}}\right) \quad (2.39)$$

$$\beta_s = -\arcsin\left(\frac{c\beta_b(ws\phi + rs\theta\dot{\phi}) + s\beta_b(wc\theta c\phi - r\dot{\theta})}{\sqrt{(wc\theta c\phi - r\dot{\theta})^2 + (ws\phi + rs\theta\dot{\phi})^2}}\right) \quad (2.40)$$

2.4 Aerodynamic forces

The unitvectors defining the wind-frame \mathcal{F}_w are given in equations (2.27)-(2.29). These will define the direction of the aerodynamic forces. Three aerodynamic forces and three moments are acting on the kite. Two of these moments are cancelled out by the cable, such that only the moment around the z-axis of the body frame is left. The forces and moments acting on the body may be summarized:

- Drag force, F_d
- Crosswind force, F_c
- Lift force, F_l
- Yawing moment, M_k

The forces have the orientation of the wind-frame:

$$F_{aer}^w = \begin{pmatrix} F_d \\ F_c \\ F_l \end{pmatrix} \quad (2.41)$$

From aerodynamics theory [10], the above forces and moments are given:

$$F_{aer}^w = \frac{1}{2}\rho_{air}w_e^2A \begin{pmatrix} C_d \\ \frac{A_c}{A}C_c \\ C_l \end{pmatrix} \quad (2.42)$$

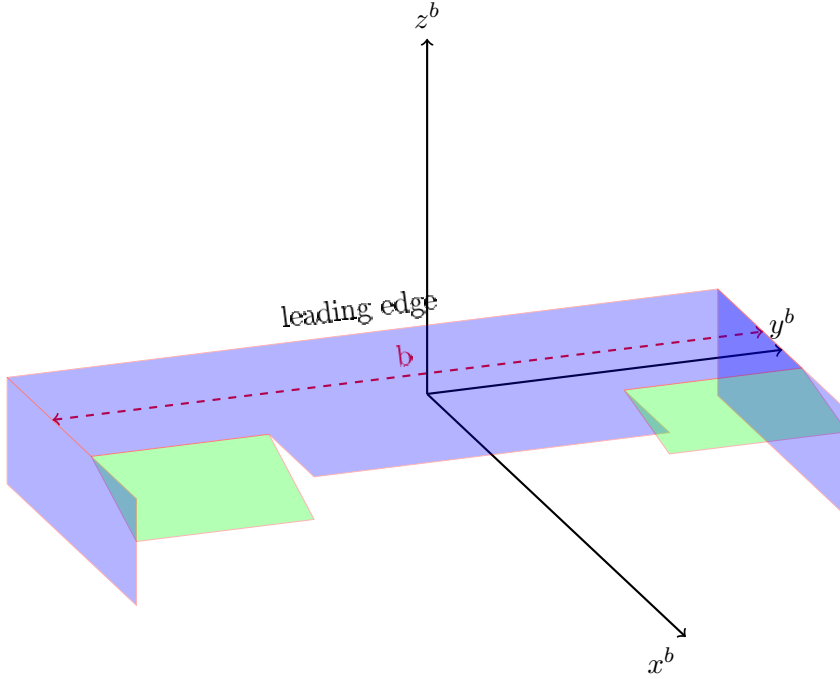


Figure 2.4: Overview of parameters and dimensions of the kite.

$$M_k = \frac{1}{2} \rho_{air} w_e^2 b A C_k - c_{kd} \dot{\beta}_b \quad (2.43)$$

Where ρ_{air} is the density of the air at the altitude of the kite, \vec{w}_e is the relative wind to the kite, A is the horizontal area, and A_c is the vertical surface area of the kite. C_d is the coefficient of drag, C_c the coefficient of crosswind force, C_l the coefficient of lift, C_k the coefficient of yawing-moment and C_{kd} the damping coefficient around the yaw axis.

All the above coefficients are variables often determined by experiments specific for an airfoil. For low speeds, and small α_w and β_s , several simplifications may be performed [14]. The aerodynamic coefficients simplified to

be functions of the following:

- Angle of attack, α_a
- Sideslip, β_s
- Control input, δ_c

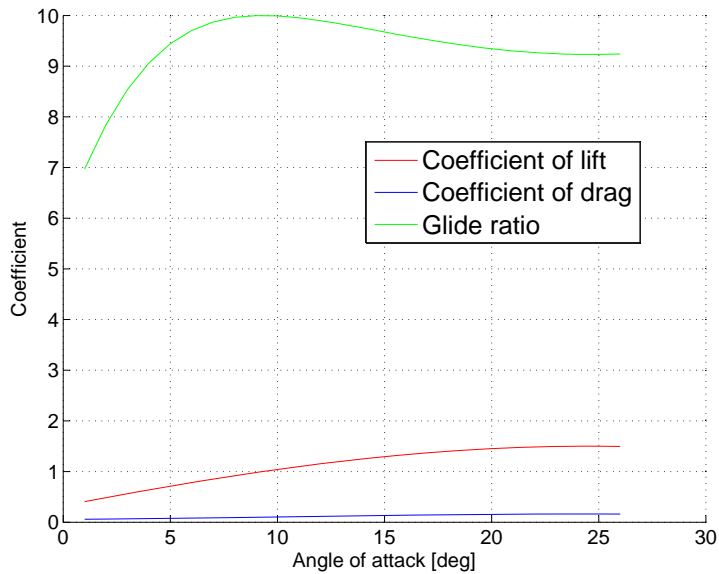


Figure 2.5: Aerodynamic coefficients and glide ratio.

Furthermore, if a symmetric airfoil is chosen, minimum lift and drag is found in $\alpha_a = 0$ [10].

It was previously stated that α_w and β_s remains relatively small. For such conditions, the coefficient of drag is approximated, [14]:

$$C_d = k_d C_l^2 + C_{dm} \quad (2.44)$$

Which is a function of the coefficient lift, where k_d is a constant and C_{dm} is the minimum drag.

The coefficient of lift is approximated:

$$C_l = C_{l,max} \sin(c_{ls}\alpha_a) \quad (2.45)$$

Where c_{ls} represents the lift slope. Because the airfoil of the kite may be configured with a constant ‘depower’- angle α_0 , the angle of attack is given:

$$\alpha_a = -\alpha_w - \alpha_0 \quad (2.46)$$

Note that the sign is negative, due to the orientation of the wind-frame. The relation between C_l and C_d , namely the glide-ratio $GR = \frac{C_l}{C_d}$, is important for the performance of an airfoil. The power output of a tethered airfoil is almost proportional to the cube of the glide-ratio [11]. Figure 2.5 shows an example of C_l , C_d and GR .

For the coefficient of the crosswind force, a linear approximation for small β_s is chosen:

$$C_c = c_{cs}\beta_s \quad (2.47)$$

The yawing moment consists of two components. There is the natural directional stability of the kite, and the flaps angle δ_l :

$$C_k = -c_{ks}\beta_s + c_{k,\delta c}\delta_l \quad (2.48)$$

where c_{ks} is the slope of C_k with respect to β_s , and $c_{k,\delta c}$ is the slope with respect to the δ_l . The final expression for the yawing-moment M_k is established:

$$M_k = \frac{1}{2}\rho_{air}w_e^2bA(-c_{ks}\beta_s + c_{k,\delta c}\delta_l) - c_{kd}\dot{\beta}_b \quad (2.49)$$

where a natural damping factor $c_{kd}\dot{\beta}_b$ is added.

The aerodynamic force for use with the state-space model is summarised:

$$F_{aer}^w = \frac{1}{2} \rho_{air} w_e^2 A \begin{pmatrix} C_d(\alpha_a) \\ \frac{A_c}{A} C_c(\beta_s) \\ C_l(\alpha_a) \end{pmatrix} \quad (2.50)$$

2.5 Kite model in state space

Starting with the kinematic model described in the previous sections:

$$\begin{pmatrix} \ddot{\theta} \\ \ddot{\phi} \\ \ddot{\beta}_b \\ \dot{\delta}_l \end{pmatrix} = \begin{pmatrix} \left(S^{-1} \frac{F^l}{m} - a \right)_1 \\ \left(S^{-1} \frac{F^l}{m} - a \right)_2 \\ \frac{M_k}{I_k} \\ b_u u \end{pmatrix} \quad (2.14)$$

the following state vector is chosen:

$$x = \begin{pmatrix} \theta \\ \phi \\ \beta_b \\ \dot{\theta} \\ \dot{\phi} \\ \dot{\beta}_b \\ \delta_l \end{pmatrix} \quad (2.51)$$

Now, the state space representation of the model is given:

$$\dot{x} = \begin{pmatrix} \dot{x}_1 \\ \dot{x}_2 \\ \dot{x}_3 \\ \dot{x}_4 \\ \dot{x}_5 \\ \dot{x}_6 \\ \dot{x}_7 \end{pmatrix} = \begin{pmatrix} x_4 \\ x_5 \\ x_6 \\ \left(S^{-1} \frac{F^l}{m} - a \right)_1 \\ \left(S^{-1} \frac{F^l}{m} - a \right)_2 \\ \frac{M_k}{I_k} \\ b_u u \end{pmatrix} = f(x, u) \quad (2.52)$$

Note that the above system only has 4 degrees of freedom, and only one control input u . Thus the system of equation (2.52) is classified as an underactuated mechanical system [13]. This classification is an important property.

Chapter 3

Control design

3.1 Introduction

Although automated control of kites is not a new concept in the academic community, limited literature on the subject is available. Several research groups have suggested the use of model predictive control to solve the problem. However, to the author best knowledge, there has not been performed any analysis using path-referencing techniques or Lyapunov theory.

The system model of equation (2.52) is classified as an underactuated system. Such systems complicates the control problem as they have severe limitations in the controllability. Tracking control and path following control has been developed both for aerial vehicles and marine vessels [3], both being underactuated systems. While these systems have actuators for translational motion, the tethered airfoil does not. If a trajectory is a path in space as a function of time, trajectory tracking would require control in translational motion. Path following on the other hand, is more suitable for controlling a tethered airfoil, as the airfoil may follow a predetermined curve in space, independently of time.

In this chapter, a control strategy for path following along a general path

on a spherical surface is proposed. The controller is inspired by the Line of Sight guidance controller suggested in [3] for underwater vessels and 3D path following in general.

3.2 Path-frame

In order to develop a path-following system, the path-error vector \vec{r}_{pb} , and the dynamics of this needs to be defined.

The Path-frame \mathcal{F}_p used in the following analysis is a geodesic reference frame [4]. Given a path \mathcal{P} parameterised by the vector $\vec{r}(s)$ where s is the position along the path. The orientation of the path-frame is defined:

$$\vec{e}_{1p} = \frac{\frac{\partial \vec{r}}{\partial s}}{\left| \frac{\partial \vec{r}}{\partial s} \right|} \quad (3.1)$$

$$\vec{e}_{2p} = \vec{e}_r \times \vec{e}_{1p} \quad (3.2)$$

$$\vec{e}_{3p} = \vec{e}_r \quad (3.3)$$

$$(3.4)$$

This reference-frame is illustrated in Figure 3.1.

In the following, the angular velocity of the earth is neglected, such that the earth-frame described in chapter 2.3 may be treated as an inertial frame. The velocity of the path-frame \vec{v}_p is given as follows:

$$\vec{v}_p = \dot{s} \vec{e}_{1p} \quad (3.5)$$

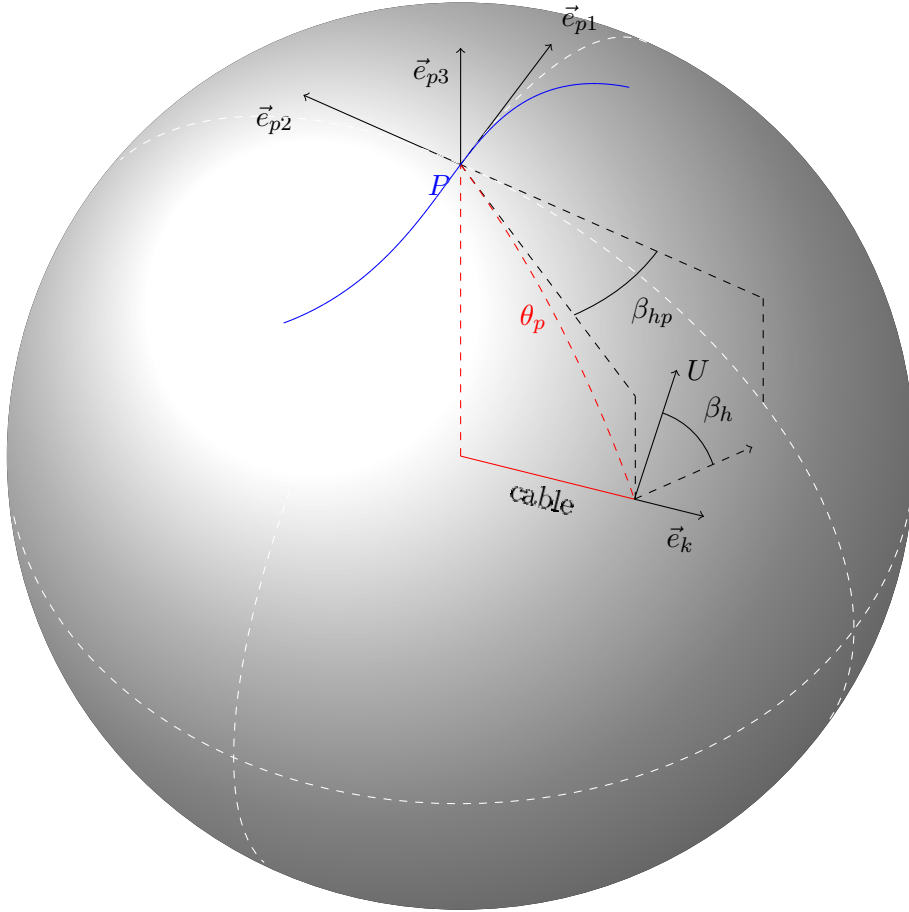


Figure 3.1: Path frame

As described in [5], the angular velocity of the path-frame is given by:

$$\omega_{ep}^p = \begin{pmatrix} \mathbf{e}_{3p}^{eT} \dot{\mathbf{e}}_{2p}^e \\ \mathbf{e}_{1p}^{eT} \dot{\mathbf{e}}_{3p}^e \\ \mathbf{e}_{2p}^{eT} \dot{\mathbf{e}}_{1p}^e \end{pmatrix} = \dot{s} \omega_{ep/s}^p \quad (3.6)$$

$$= \dot{s} \begin{pmatrix} \mathbf{e}_{3p}^{eT} \frac{\partial \mathbf{e}_{2p}^e}{\partial s} \\ \mathbf{e}_{1p}^{eT} \frac{\partial \mathbf{e}_{3p}^e}{\partial s} \\ \mathbf{e}_{2p}^{eT} \frac{\partial \mathbf{e}_{1p}^e}{\partial s} \end{pmatrix} \quad (3.7)$$

The skew symmetric matrix Ω_{ep}^p of ω_{ep}^p is used in vector products.

$$\Omega_{ep}^p = \begin{pmatrix} 0 & -\omega_{ep3}^p & \omega_{ep2}^p \\ \omega_{ep3}^p & 0 & -\omega_{ep1}^p \\ -\omega_{ep1}^p & \omega_{ep1}^p & 0 \end{pmatrix} \quad (3.8)$$

If the path-error \vec{r}_{pb} is set to be the vector from the closest point on the path \mathcal{P} to the body, it must be perpendicular to the path, meaning zero error in the x -direction:

$$\vec{r}_{bp} = y\vec{e}_{2p} + z\vec{e}_{3p} \quad (3.9)$$

Now, the velocity of the body is related to the velocity of \mathcal{F}_p .

$$\vec{v}_b = \vec{v}_p + \frac{{}^e\partial\vec{r}_{bp}}{\partial t} \quad (3.10)$$

$$= \vec{v}_p + \frac{{}^p\partial\vec{r}_{bp}}{\partial t} + \vec{\omega}_{ep} \times \vec{r}_{bp} \quad (3.11)$$

$$v_b^p = \begin{pmatrix} \dot{s} \\ 0 \\ 0 \end{pmatrix} + \begin{pmatrix} 0 \\ \dot{y} \\ \dot{z} \end{pmatrix} + \dot{s} \begin{pmatrix} 0 & -\omega_{ep/s3}^p & \omega_{ep/s2}^p \\ \omega_{ep/s3}^p & 0 & -\omega_{ep/s1}^p \\ -\omega_{ep/s2}^p & \omega_{ep/s1}^p & 0 \end{pmatrix} \begin{pmatrix} 0 \\ y \\ z \end{pmatrix} \quad (3.12)$$

Rewriting the above equation:

$$v_b^p = \begin{pmatrix} 1 - \omega_{ep/s3}^p y + \omega_{ep/s2}^p z & 0 & 0 \\ -\omega_{ep/s1}^p z & 1 & 0 \\ \omega_{ep/s1}^p y & 0 & 1 \end{pmatrix} \begin{pmatrix} \dot{s} \\ \dot{y} \\ \dot{z} \end{pmatrix} \quad (3.13)$$

The above differential equation describes the relation between the velocity of the kite and the Path-frame. It also describes the distance between the path and the body as a function of time. However, there is a singularity in the right hand matrix, for:

$$1 - \omega_{ep/s3}^p y + \omega_{ep/s2}^p z = 0 \quad (3.14)$$

As suggested in [3], this may be solved by adding dynamics to the origin of the Path-frame. The relative position of the body-frame to the path-frame is redefined:

$$\vec{r}_{pb} = x\vec{e}_{1p} + y\vec{e}_{2p} + z\vec{e}_{3p} \quad (3.15)$$

This is inserted into equation (3.12):

$$v_b^p = \begin{pmatrix} \dot{s} \\ 0 \\ 0 \end{pmatrix} + \begin{pmatrix} \dot{x} \\ \dot{y} \\ \dot{z} \end{pmatrix} + \dot{s} \begin{pmatrix} 0 & -\omega_{ep/s3}^p & \omega_{ep/s2}^p \\ \omega_{ep/s3}^p & 0 & -\omega_{ep/s1}^p \\ -\omega_{ep/s2}^p & \omega_{ep/s1}^p & 0 \end{pmatrix} \begin{pmatrix} x \\ y \\ z \end{pmatrix} \quad (3.16)$$

To cancel out the singularity, the x-dynamics is chosen:

$$\dot{x} = -k_x x + \omega_{ep/s3}^p y - \omega_{ep/s2}^p z \quad (3.17)$$

where $k_x > 0$ such that $x = 0$ is exponentially stable when $y = z = 0$. Equations (3.16) and (3.17) are rewritten to obtain state-space form:

$$\begin{pmatrix} 1 - \omega_{ep/s3}^p y + \omega_{ep/s2}^p z & 0 & 0 & 1 \\ \omega_{ep/s3}^p x - \omega_{ep/s1}^p z & 1 & 0 & 0 \\ -\omega_{ep/s2}^p x + \omega_{ep/s1}^p y & 0 & 1 & 0 \\ -\omega_{ep/s3}^p y + \omega_{ep/s2}^p z & 0 & 0 & 1 \end{pmatrix} \begin{pmatrix} \dot{s} \\ \dot{y} \\ \dot{z} \\ \dot{x} \end{pmatrix} = \begin{pmatrix} v_b^p \\ -k_x x \end{pmatrix} \quad (3.18)$$

The determinant is investigated,

$$\begin{aligned} \det \begin{pmatrix} 1 - \omega_{ep/s3}^p y + \omega_{ep/s2}^p z & 0 & 0 & 1 \\ \omega_{ep/s3}^p x - \omega_{ep/s1}^p z & 1 & 0 & 0 \\ -\omega_{ep/s2}^p x + \omega_{ep/s1}^p y & 0 & 1 & 0 \\ -\omega_{ep/s3}^p y + \omega_{ep/s2}^p z & 0 & 0 & 1 \end{pmatrix} \\ = \left(1 - \omega_{ep/s3}^p y + \omega_{ep/s2}^p z\right) - \left(-\omega_{ep/s3}^p y + \omega_{ep/s2}^p z\right) = 1 \end{aligned} \quad (3.19)$$

which proves the singularity of Equation (3.13) has been corrected. Equation (3.18) describes the path-error development in time, as a function of the body-velocity. This is an important result in developing the path-following controller.

3.3 The movement-frame

Equation (3.18) relates the path-error development to the body velocity given in the path frame. A few assumptions is made on the system (2.52) before defining the relation between the two frames.

Assumption 1 The kite is operated in a manner such that the total velocity U is bounded: $U_{min} \leq U \leq U_{max}$.

Assumption 2 The sideslip angle $\beta_{h,s} = \beta_h - \beta_b$ where $\beta_h = \arctan\left(\frac{\dot{\phi} \sin(\theta)}{\dot{\theta}}\right)$ is less than 90° : $|\beta_{h,s}| < 90^\circ$, and $|\dot{\beta}_{h,s}| < \dot{\beta}_{s,max}$

Assumption 3 The heading β_h is controllable through the yawing angle β_b .

By defining a movement frame \mathcal{F}_m , with the velocity $\|v\| = U = \sqrt{v_1^2 + v_2^2 + v_3^2}$ in the direction of the first axis \vec{e}_{m1} , such that $v_b^m = (U \ 0 \ 0)^T$, the rotation between \mathcal{F}_m and \mathcal{F}_p is given:

$$\begin{aligned} R_m^p &= R_3(\beta_p)R_1(\theta_p)R_3(\beta_{hp}) \\ &= \begin{pmatrix} c\beta_p c\beta_{hp} - s\beta_p c\theta_p s\beta_{hp} & c\beta_p s\beta_{hp} + s\beta_p c\theta_p c\beta_{hp} & s\beta_p s\theta_p \\ -s\beta_p c\beta_{hp} - c\beta_p c\theta_p s\beta_{hp} & -s\beta_p s\beta_{hp} + c\beta_p c\theta_p c\beta_{hp} & c\beta_p s\theta_p \\ s\theta_p s\beta_{hp} & -s\theta_p c\beta_{hp} & c\theta_p \end{pmatrix} \end{aligned} \quad (3.20)$$

The three angles of rotation β_p , θ_p and β_{hp} are illustrated in the Figure 3.1. The body velocity $\mathbf{u}_b^m = (U \ 0 \ 0)^T$, given in the path-frame is calculated:

$$R_m^p \mathbf{u}_b^m = U \begin{pmatrix} c\beta_p c\beta_{hp} - s\beta_p c\theta_p s\beta_{hp} \\ -s\beta_p c\beta_{hp} - c\beta_p c\theta_p s\beta_{hp} \\ s\theta_p s\beta_{hp} \end{pmatrix} \quad (3.21)$$

In the above rotation matrices, for the ease of notation, s and c is used for sin and cos. While the angles β_p and θ_p are functions of the relative position

between the body and the origin of the path-frame, β_{hp} is controllable. By geometric relations, the angles β_p and θ_p are defined:

$$\beta_p = \begin{cases} 0 & \text{for } x, y = 0 \\ \arctan\left(\frac{x}{y}\right) & \text{elsewhere} \end{cases} \quad (3.22)$$

$$\theta_p = \operatorname{sgn}(y) \arccos\left(\frac{r+z}{r}\right) = \operatorname{sgn}(y) \arcsin\left(\frac{\sqrt{x^2+y^2}}{r}\right) \quad (3.23)$$

Note that either of these representations for θ_p may be chosen in the following calculations.

3.4 Path error in cartesian coordinates

As previously stated, both the origin of the path-frame and the body-frame is at all times positioned on the same spherical surface. This surface is defined by the distance r from the origin of the earth-frame. By this, a set \mathcal{D} is defined: $\mathcal{D} = \left\{ r_{bp} \in \mathcal{R}^3 \rightarrow \mathcal{R}^2 \mid x^2 + y^2 \leq r^2 \cap z = -r \pm \sqrt{r^2 - x^2 - y^2} \right\}$ such that $\mathbf{r}_{bp} = (x \ y \ z)^T$ is the vector from the path-frame to the body frame. Any trajectories of the following system will allways stay in \mathcal{D} .

The xyz-statespace equations of the path error in Equation (3.18) is defined:

$$\dot{x} = -k_x x + \dot{s} \omega_{ep/s3}^p y - \dot{s} \omega_{ep/s2}^p z \quad (3.24)$$

$$\dot{y} = (R_m^p v_b^m)_2 - \dot{s} \omega_{ep/s3}^p x + \dot{s} \omega_{ep/s1}^p z \quad (3.25)$$

$$\dot{z} = (R_m^p v_b^m)_3 + \dot{s} \omega_{ep/s2}^p x - \dot{s} \omega_{ep/s1}^p y \quad (3.26)$$

Now, standard form is obtained:

$$\begin{pmatrix} \dot{x} \\ \dot{y} \\ \dot{z} \end{pmatrix} = \begin{pmatrix} -k_x x \\ (R_m^p v_b^m)_2 \\ (R_m^p v_b^m)_3 \end{pmatrix} + \dot{s} \begin{pmatrix} 0 & \omega_{ep/s3}^p & -\omega_{ep/s2}^p \\ -\omega_{ep/s3}^p & 0 & \omega_{ep/s1}^p \\ \omega_{ep/s2}^p & -\omega_{ep/s1}^p & 0 \end{pmatrix} \begin{pmatrix} x \\ y \\ z \end{pmatrix} \quad (3.27)$$

where the skew symmetric property of the last term becomes clear. The rotation matix $R_m^p(\beta, \theta_p, \beta_{hp})$ is given in Equation (3.21), where β_{hp} is the only controllable variable. For now, it is assumed that β_{hp} is controlled to some desired value $\beta_{hp,d}$, with some error $\tilde{\beta}_{hp} = \beta_{hp} - \beta_{hp,d}$. Inserting this into the above equation yields:

$$\begin{pmatrix} \dot{x} \\ \dot{y} \\ \dot{z} \end{pmatrix} = \begin{pmatrix} -k_x x \\ -U s \beta_p c \beta_{hp,d} - U c \beta_p c \theta s \beta_{hp,d} \\ U s \theta s \beta_{hp,d} \end{pmatrix} + \dot{s} \begin{pmatrix} 0 & \omega_{ep/s3}^p & -\omega_{ep/s2}^p \\ -\omega_{ep/s3}^p & 0 & \omega_{ep/s1}^p \\ \omega_{ep/s2}^p & -\omega_{ep/s1}^p & 0 \end{pmatrix} \begin{pmatrix} x \\ y \\ z \end{pmatrix} + \mathbf{g}(x, y, z, \tilde{\beta}_h) \tilde{\beta}_h \quad (3.28)$$

A compact form of Equation (3.28) states the path-error system:

$$\dot{\mathbf{z}}_1 = \mathbf{f}_1(\mathbf{z}_1) + \mathbf{g}(\mathbf{z}_1)z_2 \quad (3.29)$$

Where $\mathbf{z}_1 = \mathbf{r}_{bp}$, $z_2 = \tilde{\beta}_h = \beta_h - \beta_{hp,d}$, and \mathbf{g} is the error gain vector:

$$\mathbf{g}(x, y, z, \tilde{\beta}_h) = \begin{pmatrix} g_1 \\ g_2 \\ g_3 \end{pmatrix} \quad (3.30)$$

$$g_1 = 0 \quad (3.31)$$

$$g_2 = U \left(s\beta_p \frac{s\beta_{hp,d}s\tilde{\beta}_h + (c\tilde{\beta}_h - 1)c\beta_{hp,d}}{\tilde{\beta}_h} - c\beta_p c\theta_p \frac{c\beta_{hp,d}s\tilde{\beta}_h + (c\tilde{\beta}_h - 1)s\beta_{hp,d}}{\tilde{\beta}_h} \right) \quad (3.32)$$

$$g_3 = Us\theta_p \frac{c\beta_{hp,d}s\tilde{\beta}_h + (c\tilde{\beta}_h - 1)s\beta_{hp,d}}{\tilde{\beta}_h} \quad (3.33)$$

Where g_2 and g_3 are bounded above:

$$\lim_{\tilde{\beta}_h \rightarrow 0} \frac{c\tilde{\beta}_h - 1}{\tilde{\beta}_h} = 0 \quad (3.34)$$

$$\lim_{\tilde{\beta}_h \rightarrow 0} \frac{s\tilde{\beta}_h}{\tilde{\beta}_h} = 1 \quad (3.35)$$

By this result, the system in Equation (3.29) is interpreted as the nominal system $\dot{\mathbf{z}}_1 = \mathbf{f}_1(\mathbf{z}_1)$, perturbed by the error \mathbf{z}_2 through the error gain vector $\mathbf{g}(\mathbf{z}_1)$.

3.5 Path following system

The path error development of the nominal system in equation (3.28) is given:

$$\begin{pmatrix} \dot{x} \\ \dot{y} \\ \dot{z} \end{pmatrix} = \begin{pmatrix} -k_x x \\ -Us\beta_p c\beta_{h,d} - Uc\beta_p c\theta s\beta_{h,d} \\ Us\theta s\beta_{h,d} \end{pmatrix} + \dot{s} \begin{pmatrix} 0 & \omega_{ep/s3}^p & -\omega_{ep/s2}^p \\ -\omega_{ep/s3}^p & 0 & \omega_{ep/s1}^p \\ \omega_{ep/s2}^p & -\omega_{ep1/s}^p & 0 \end{pmatrix} \begin{pmatrix} x \\ y \\ z \end{pmatrix} \quad (3.36)$$

In the above system, $\beta_{h,d}$ may be designed to make the origin $(x \ y \ z)^T = (0 \ 0 \ 0)^T$ a stable equilibrium point.

3.5.1 Guidance law

The guidance law presented in [3] is proven to stabilize the vehicle to a path-frame using a Line of Sight-technique(LOS). LOS means aiming at some point $(\Delta \ 0 \ 0)^T$ ahead of the centre of the path-frame. In the case with spherical coordinates, this is not possible. Inspired by this, an aiming angle along the arc between the body- and the path-frame is chosen. This is illustrated in Figure 3.1.

$$\begin{aligned} \beta_{hp,d} &= \beta_{h,\Delta} - \beta_p \\ &= \begin{cases} 0 & \text{for } x, y = 0 \\ \arctan\left(\frac{y}{\Delta}\right) - \arctan\left(\frac{x}{y}\right) & \text{elsewhere} \end{cases} \end{aligned} \quad (3.37)$$

3.5.2 Stability analysis of the nominal system

Now that all the angles of rotation between the movement-frame and the path-frame is defined, a stability analysis for the nominal system may be

$\sin(\arctan x) = \frac{x}{\sqrt{x^2+1}}$
$\cos(\arctan x) = \frac{1}{\sqrt{x^2+1}}$
$\sin(\arccos x) = \sqrt{1-x^2}$
$\cos(\arcsin x) = \sqrt{1-x^2}$

Table 3.1: Trigonometric relations

performed. The three angles of rotation are given in Equations (3.22), (3.23) and (3.37).

$$\beta_p = \begin{cases} 0 & \text{for } x, y = 0 \\ \arctan\left(\frac{x}{y}\right) & \text{elsewhere} \end{cases} \quad (3.22)$$

$$\theta_p = \operatorname{sgn}(y) \arccos\left(\frac{r+z}{r}\right) = \operatorname{sgn}(y) \arcsin\left(\frac{\sqrt{x^2+y^2}}{r}\right) \quad (3.23)$$

By using the trigonometric relations listed in Table 3.1, the sines and cosines of the three angles are calculated.

$$\begin{aligned} \sin(\beta_{h,d}) &= s\beta_{h,\Delta}c\beta_p - c\beta_{h,\Delta}s\beta_p \\ &= \frac{y}{\sqrt{y^2+\Delta^2}} \frac{|y|}{\sqrt{x^2+y^2}} - \frac{\Delta}{\sqrt{y^2+\Delta^2}} \frac{\operatorname{sgn}(y)x}{\sqrt{x^2+y^2}} \end{aligned} \quad (3.38)$$

$$\begin{aligned} \cos(\beta_{h,d}) &= c\beta_{h,\Delta}c\beta_p + s\beta_{h,\Delta}s\beta_p \\ &= \frac{\Delta}{\sqrt{y^2+\Delta^2}} \frac{|y|}{\sqrt{x^2+y^2}} + \frac{y}{\sqrt{y^2+\Delta^2}} \frac{\operatorname{sgn}(y)x}{\sqrt{x^2+y^2}} \end{aligned} \quad (3.39)$$

$$\sin(\theta_p) = \operatorname{sgn}(y) \frac{\sqrt{x^2+y^2}}{r} \quad (3.40)$$

$$\cos(\theta_p) = \frac{r+z}{r} \quad (3.41)$$

$$\sin(\beta_p) = \frac{\operatorname{sgn}(y)x}{\sqrt{x^2+y^2}} \quad (3.42)$$

$$\cos(\beta_p) = \frac{|y|}{\sqrt{x^2+y^2}} \quad (3.43)$$

The above expressions is inserted into equation (3.36)

$$\dot{x} = -k_x x + (S_M \mathbf{z}_1)_1 \quad (3.44)$$

$$\begin{aligned} \dot{y} &= U \left(-\frac{\text{sgn}(y)x}{\sqrt{x^2 + y^2}} \left(\frac{\Delta}{\sqrt{y^2 + \Delta^2}} \frac{|y|}{\sqrt{x^2 + y^2}} + \frac{y}{\sqrt{y^2 + \Delta^2}} \frac{\text{sgn}(y)x}{\sqrt{x^2 + y^2}} \right) \right. \\ &\quad \left. - \frac{|y|}{\sqrt{x^2 + y^2}} \frac{r+z}{r} \left(\frac{y}{\sqrt{y^2 + \Delta^2}} \frac{|y|}{\sqrt{x^2 + y^2}} - \frac{\Delta}{\sqrt{y^2 + \Delta^2}} \frac{\text{sgn}(y)x}{\sqrt{x^2 + y^2}} \right) \right) \\ &\quad + (S_M \mathbf{z}_1)_2 \\ &= U \frac{-r\Delta xy - rx^2y - (r+z)|y|^2y + (r+z)\Delta xy^2}{r(x^2 + y^2)\sqrt{y^2 + \Delta^2}} + (S_M \mathbf{z}_1)_2 \\ &= U \frac{-rx^2y - (r+z)|y|^2y + z\Delta xy}{r(x^2 + y^2)\sqrt{y^2 + \Delta^2}} + (S_M \mathbf{z}_1)_2 \end{aligned} \quad (3.45)$$

$$\begin{aligned} \dot{z} &= U \left(\text{sgn}(y) \frac{\sqrt{x^2 + y^2}}{r} \left(\frac{y}{\sqrt{y^2 + \Delta^2}} \frac{|y|}{\sqrt{x^2 + y^2}} - \frac{\Delta}{\sqrt{y^2 + \Delta^2}} \frac{\text{sgn}(y)x}{\sqrt{x^2 + y^2}} \right) \right) \\ &\quad + (S_M \mathbf{z}_1)_3 \\ &= U \frac{y^2 - \Delta x}{r\sqrt{y^2 + \Delta^2}} + (S_M \mathbf{z}_1)_3 \end{aligned} \quad (3.46)$$

Where the origin $\mathbf{z}_1 = \mathbf{0}$ is an equilibrium point:

$$\lim_{x \rightarrow 0} \bigg|_{y=0} \dot{\mathbf{z}}_1 = \lim_{y \rightarrow 0} \bigg|_{x=0} \dot{\mathbf{z}}_1 = 0 \quad (3.47)$$

Now, a Lyapunov analysis of the nominal system in Equations (3.44) - (3.46) is performed, using the following Lyapunov function candidate:

$$V_{nom} = \frac{1}{2} \mathbf{z}_1^T \mathbf{z}_1 = \frac{1}{2} (x \quad y \quad z) \begin{pmatrix} x \\ y \\ z \end{pmatrix} \quad (3.48)$$

The first derivative is calculated:

$$\begin{aligned}
\dot{V}_{nom} &= (x \quad y \quad z) \begin{pmatrix} \dot{x} \\ \dot{y} \\ \dot{z} \end{pmatrix} \\
&= (x \quad y \quad z) \begin{pmatrix} -k_x x \\ U \frac{-rx^2y - (r+z)|y|^2y + z\Delta xy}{r(x^2+y^2)\sqrt{y^2+\Delta^2}} \\ U \frac{y^2 - \Delta x}{r\sqrt{y^2+\Delta^2}} \end{pmatrix} \\
&\quad + \cancel{\frac{\dot{\omega}^p}{ep/s3}xy} - \cancel{\frac{\dot{\omega}^p}{ep/s2}xz} - \cancel{\frac{\dot{\omega}^p}{ep/s3}xy} + \cancel{\frac{\dot{\omega}^p}{ep/s1}yz} \\
&\quad + \cancel{\frac{\dot{\omega}^p}{ep/s2}xz} - \cancel{\frac{\dot{\omega}^p}{ep/s1}yz} \tag{3.49}
\end{aligned}$$

The skew symmetric terms in the above equation are conveniently cancelled out.

$$\begin{aligned}
\dot{V}_{nom} &= -k_x x^2 + \left(U \frac{-rx^2y - (r+z)|y|^2y + z\Delta xy}{r(x^2+y^2)\sqrt{y^2+\Delta^2}} \right) y + \left(U \frac{y^2 - \Delta x}{r\sqrt{y^2+\Delta^2}} \right) z \\
&= -k_x x^2 + U \frac{-rx^2y^2 - (r+z)|y|^2y^2 + z\Delta xy^2 + (x^2+y^2)(zy^2 - \Delta xz)}{r(x^2+y^2)\sqrt{y^2+\Delta^2}} \\
&= -k_x x^2 + \frac{-rx^2y^2 - ry^4 - zy^4 + \cancel{\Delta zxy^2} + zx^2y^2 - \Delta zx^3 + \cancel{zy^4} - \cancel{\Delta zxy^2}}{r(x^2+y^2)\sqrt{y^2+\Delta^2}} \\
&= -k_x x^2 + U \frac{zx^2y^2 - r(x^2+y^2)y^2 - \Delta zx^3}{r(x^2+y^2)\sqrt{y^2+\Delta^2}} \tag{3.50}
\end{aligned}$$

$$\leq \left(U \frac{-\Delta zx}{r(x^2+y^2)\sqrt{y^2+\Delta^2}} - k_x \right) x^2 \tag{3.51}$$

For the upper part of the sphere \mathcal{D} , i.e. $\mathcal{D}_{upper} = \{\mathbf{z}_1 \in \mathcal{D} \mid -r \leq z \leq 0\}$, z is given by $z = -r + \sqrt{r^2 - x^2 - y^2}$.

$$\dot{V}_{nom} \leq \left(U \frac{\Delta(r - \sqrt{r^2 - x^2 - y^2})x}{r(x^2 + y^2)\sqrt{y^2 + \Delta^2}} - k_x \right) x^2 \quad (3.52)$$

Where if $y = 0$, $\lim_{x \rightarrow 0} \frac{(r - \sqrt{r^2 - x^2 - y^2})x}{r(x^2 + y^2)} = 0$. Under the assumption that the velocity of the kite is bounded, $U_{min} \leq U \leq U_{max}$, the above expression is maximized in the set \mathcal{D}_{upper} , and the following is obtained:

$$\dot{V}_{nom} \leq \left(\frac{U_{max}}{r} - k_x \right) x^2 \leq 0 \mid_{k_x > \frac{U_{max}}{r}} \quad \forall \mathbf{z}_1 \in \mathcal{D}_{upper} \quad (3.53)$$

This proves that \dot{V}_{nom} is negative semi definite in \mathcal{D}_{upper} . Before stability is concluded, the same analysis is performed for the the lower part of the sphere: $\mathcal{D}_{lower} = \{\mathbf{z}_1 \in \mathcal{D} \mid -2r \leq z < -r\}$, z is given by $z = -r - \sqrt{r^2 - x^2 - y^2}$.

$$\dot{V}_{nom} \leq \left(U_{max} \frac{\Delta(r + \sqrt{r^2 - x^2 - y^2})x}{r(x^2 + y^2)\sqrt{y^2 + \Delta^2}} - k_x \right) x^2 \quad (3.54)$$

Again, if $y = 0$, $\lim_{x \rightarrow 0} U \frac{\Delta(r + \sqrt{r^2 - x^2 - y^2})x}{r(x^2 + y^2)\sqrt{y^2 + \Delta^2}} \rightarrow \infty$, thus there is no constant k_x to keep the above equation negative semi definite. Now a subset Ω_c is defined:

$$\Omega_c = \{\mathbf{z}_1 \in \mathcal{R}^3 \mid V(\mathbf{z}_1) \leq (2r - \delta)^2\} \subset \mathcal{D} \quad (3.55)$$

where $\delta > 0$ is some small positive number. The set Ω_c excludes a small circular area around the point $(x \ y \ z)^T = (0 \ 0 \ -2r)^T$, such that for $z \leq -r$, $x^2 + y^2 \geq r_c(\delta)^2$. This is illustrated in Figure 3.2. Using these properties, Equation (3.54) is maximised in Ω_c :

$$\dot{V}_{nom} \leq \left(U_{max} \frac{r - \sqrt{r^2 - r_c^2}}{r r_c} - k_x \right) x^2 \quad (3.56)$$

$$\dot{V} \leq (k_c - k_x) x^2 \leq 0 \Big|_{k_x > k_c} \quad \forall \mathbf{z}_1 \in \Omega_c \quad (3.57)$$

where,

$$k_c = \max \left(\frac{U_{max}}{r}, U_{max} \frac{r - \sqrt{r^2 - r_c^2}}{rr_c} \right) \quad (3.58)$$

Now the recent results are inserted into equation (3.50):

$$\dot{V}_{nom} \leq -(k_x - k_c)x^2 + U \frac{zx^2y^2}{r(x^2 + y^2)\sqrt{y^2 + \Delta^2}} - U \frac{y^2}{\sqrt{y^2 + \Delta^2}} \quad (3.59)$$

$$\boxed{\dot{V}_{nom} \leq 0 \quad \forall \mathbf{z}_1 \in \Omega_c} \quad (3.60)$$

Going back to the hard relation between z and x, y , $z = -r \pm \sqrt{r^2 - x^2 - y^2}$, it is seen that any nonzero z gives a nonzero x, y . Thus the set $\{\dot{V}_{nom} = 0\} \subset \Omega_c$ contains no other trajectories than the trivial solution $\mathbf{z}_1(t) = \mathbf{0} \forall t \geq 0$. By LaSalle's invariance principle, the equilibrium point $\mathbf{z}_1 = \mathbf{0}$ is a Locally Asymptotically Stable (LAS) equilibrium point of the system (3.36) in the set Ω_c .

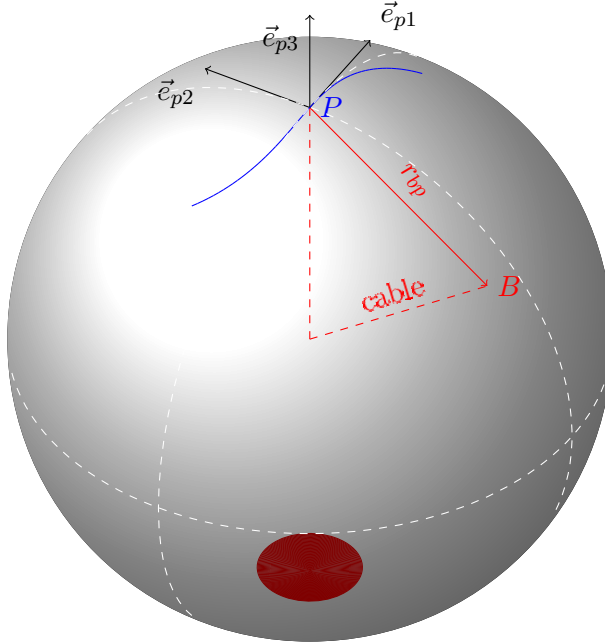


Figure 3.2: Visualization of the set Ω_c . Ω_c is given by the surface of this sphere, excluding the red area on the opposite side of the origin of the path-frame, where the path-error system is not proven stable.

3.6 Controller dynamics

Although the kite-model is an underactuated system, a combination of the states may still be influenced. For instance, the combination of $\dot{\theta}$ and $\dot{\phi}$ where the heading angle is defined $\beta_h = \arctan\left(\frac{\dot{\phi} \sin(\theta)}{\dot{\theta}}\right)$ is controllable. In the following synthesis, the backstepping method will be used until the control input is available.

The nominal system of the path error $\mathbf{z}_1 = r_{bp} = (x \ y \ z)^T$ is defined:

$$\dot{\mathbf{z}}_1 = f_1(\mathbf{z}_1) \quad (3.61)$$

$$V_{nom} = \frac{1}{2} \mathbf{z}_1^T \mathbf{z}_1 \quad (3.62)$$

$$\dot{V}_{nom} = -W(\mathbf{z}_1) \quad (3.63)$$

Where $W(\mathbf{z}_1)$ is a positive semi-definite function. The full system with a corresponding Lyapunov function is given:

$$\dot{\mathbf{z}}_1 = f_1(\mathbf{z}_1) + g_1(\mathbf{z}_1)z_2 \quad (3.64)$$

$$V_1 = \frac{1}{2} \mathbf{z}_1^T \mathbf{z}_1 \quad (3.65)$$

$$\dot{V}_1 = -W(\mathbf{z}_1) + g_1(\mathbf{z}_1)^T \mathbf{z}_1 z_2 \quad (3.66)$$

where $z_2 = \tilde{\beta} = \beta_h - \beta_{h,d} = \beta_b - \beta_{b,d}$. The heading error z_2 is included in a second Lyapunov function.

$$V_2 = V_1 + \frac{1}{2} z_2^T z_2 \quad (3.67)$$

$$\dot{V}_2 = -W(\mathbf{z}_1) + g_1(\mathbf{z}_1)^T \mathbf{z}_1 z_2 + z_2(\dot{\beta}_b - \dot{\beta}_{b,d}) \quad (3.68)$$

The control error is defined $z_3 = \dot{\beta}_b - \alpha_1$ where α_1 is a stabilizing term to decide.

$$z_3 = \dot{\beta}_b - \alpha_1 \quad \rightarrow \quad \dot{\beta}_b = z_3 + \alpha_1 \quad (3.69)$$

Inserting $\dot{\beta}$ into Equation (3.68) yields :

$$\dot{V}_2 = -W(\mathbf{z}_1) + g_1(\mathbf{z}_1)^T \mathbf{z}_1 z_2 + z_2(z_3 + \alpha_1 - \dot{\beta}_{h,d}) \quad (3.70)$$

Now, α_1 may be chosen to cancel out any perturbing terms:

$$\alpha_1 = -g_1(\mathbf{z}_1)^T \mathbf{z}_1 + \dot{\beta}_{h,d} - K z_2 \quad (3.71)$$

$$\begin{aligned} \dot{V}_2 &= -W(\mathbf{z}_1) + g_1(\mathbf{z}_1)^T \mathbf{z}_1 z_2 + z_2 \left(z_3 - g_1(\mathbf{z}_1) \mathbf{z}_1 + \dot{\beta}_{h,d} - K z_2 - \dot{\beta}_{h,d} \right) \\ & \quad (3.72) \end{aligned}$$

$$= -W(\mathbf{z}_1) - K_1 z_2^2 + z_2 z_3 \quad (3.73)$$

Another step is added to the backstepping method, using $z_3 = \dot{\beta}_b - \alpha$ and $\dot{z}_3 = \ddot{\beta}_b - \dot{\alpha}_1$:

$$V_3 = V_2 + \frac{1}{2}z_3^2 \quad (3.74)$$

$$\dot{V}_3 = -W(\mathbf{z}_1) - K_1z_2^2 + z_2z_3 + z_3 \left(\ddot{\beta}_b - \dot{\alpha}_1 \right) \quad (3.75)$$

where $\ddot{\beta}_b$ is recognised from the kite model. Equation (2.49) defines the dynamics of β_b :

$$\ddot{\beta}_b = \frac{1}{2I_k} \rho_{air} w_e^2 b A_c (-c_{ks} \beta_s + c_{k,\delta c} \delta_l) - c_{kd} \dot{\beta}_b \quad (3.76)$$

For simplicity, the above equation is rewritten.

$$\ddot{\beta}_b = \omega_1 + \omega_2 \delta_l - c_{kd} \dot{\beta}_b \quad (3.77)$$

Where the functions ω_1 and ω_2 are function of the wind vector ω and the state vector x .

$$\dot{V}_3 = -W(\mathbf{z}_1) - K_1z_2^2 + z_2z_3 + z_3 \left(\omega_1 + \omega_2 \delta_l - c_{kd} \dot{\beta}_b - \dot{\alpha}_1 \right) \quad (3.78)$$

As recalled from Equation (2.52), the relation between the flaps angle δ_l and the control input is simple, $\dot{\delta}_l = u$. This state is easily controlled by some high speed actuator.

Further assumptions are made.

Assumption 4 ω_1 and ω_2 are known, positive, bounded scalar functions.

Assumption 5 The state δ_l is controlled perfectly to a desired $\delta_{l,d}$, that is

$$\delta_l = \delta_{l,d}$$

Now, δ_l may be considered a control input to the system.

$$\boxed{\delta_{l,d} = \frac{1}{\omega_2} \left(-z_2 - \omega_1 + c_{kd} \dot{\beta}_b + \dot{\alpha}_1 - K_2 z_3 \right)} \quad (3.79)$$

Inserting this into Equation (3.78), the following final result is obtained:

$$\boxed{\dot{V}_3 = -W(\mathbf{z}_1) - K_1 z_2^2 - K_2 z_3^2} \quad (3.80)$$

Because $\dot{V}_3 = \dot{V}_1 - W_1(z_2, z_3)$ where W_1 is a positive definite function, it is concluded for the path error system in Equation (3.27) that the origin is Locally Asymptotically Stable (LAS).

Although the above result is conclusive, it underlies some assumptions. ω_1 and ω_2 are function of the wind vector ω and the states. Accurate state estimates are likely to be available, while the wind is a random process. Some error will occur in the estimates of ω_1 and ω_2 . The term $\dot{\alpha}_1$ contains the second derivative of $\beta_{h,d}$, $\ddot{\beta}_{h,d}$. When designing a curve in space, keeping $\ddot{\beta}_{h,d}$ continuous, is a limitation.

Despite the fact that the controller proposed in Equation (3.79) contains a few weaknesses, it is a solid result. The controller is, -to the authors best knowledge-, the first to solve the problem of general path-following for tethered airfoils, in ideal conditions.

Chapter 4

Simulation

4.1 Introduction

The following simulations demonstrate a single tethered airfoil fixed to a stationary point on the ground. As the scope of this thesis is not to investigate the optimality in different trajectories with respect to power generation, the path is chosen to facilitate analytical calculations, and to demonstrate the concept of path-following control.

4.2 Parametric curve in spherical coordinates

The purpose of the following curve, is to demonstrate the control system developed in this thesis. The curve is not optimised by any means, but is designed to resemble a *figure eight*-shaped path. Such a flight pattern is supported by several analysts in the field,[6], [8], and is a well known technique for manoeuvring tethered airfoils. A parametric curve $\gamma(\zeta)$ is defined: $\gamma(\zeta) = (\theta_p(\zeta) \phi(\zeta) r)^T$, and the velocity of this with respect to ζ , $\gamma'_v(\zeta) = S\gamma'(\zeta)$ where S is a scaling matrix due to the use of spherical

coordinates. $\gamma'_v(\zeta)$ is the parametric velocity in the local frame.

$$\gamma'_v(\zeta) = \frac{s_t}{2\pi} \begin{pmatrix} \cos(2\zeta) \\ |\sin(2\zeta)| \operatorname{sgn}(\sin(\zeta)) \\ 0 \end{pmatrix} \quad \forall \quad \zeta \in [0, 2\pi] \quad (4.1)$$

$$= \begin{pmatrix} r & 0 & 0 \\ 0 & r \sin(\theta) & 0 \\ 0 & 0 & 1 \end{pmatrix} \begin{pmatrix} \theta'(\zeta) \\ \phi'(\zeta) \\ r'(\zeta) \end{pmatrix} \quad (4.2)$$

In the above equation, s_t is the total length of the closed curve. The desired parameterisation of the curve γ , is $\gamma(s)$. To reparameterise, the distance s travelled along the curve γ is calculated, [7]:

$$s(\zeta) = \int_0^\zeta |\gamma'_v(t)| dt \quad (4.3)$$

$$= \int_0^\zeta \frac{s_t}{2\pi} \sqrt{\cos^2(2t) + \sin^2(2t)} dt \quad (4.4)$$

$$= \frac{s_t}{2\pi} \zeta \quad (4.5)$$

$$\zeta = 2\pi \frac{s}{s_t} \quad (4.6)$$

Now, a substitution between ζ and s can be made. The expressions $\theta(s)$, $\phi(s)$ and $r(s)$ may be calculated using equations (4.1)-(4.2), and substituting ζ with s .

$$\frac{\partial \theta_p}{\partial s} = \cos \left(4\pi \frac{s}{s_t} \right) \quad (4.7)$$

$$\frac{\partial \phi_p}{\partial s} = \frac{|\sin(4\pi \frac{s}{s_t})| \operatorname{sgn}(\sin(2\pi \frac{s}{s_t}))}{r \sin \left(\frac{s_t}{4\pi r} \sin \left(4\pi \frac{s}{s_t} \right) + \theta_0 \right)} \quad (4.8)$$

$$\frac{\partial r}{\partial s} = 0 \quad (4.9)$$

$$\theta(s) = \frac{st}{4\pi r} \sin(4\pi \frac{s}{s_t}) + \theta_0 \quad (4.10)$$

$$\phi(s) = \int_0^{2\pi \frac{s}{s_t}} \frac{|\sin(2t)| \operatorname{sgn}(\sin(t))}{r \sin(\frac{st}{4\pi r} \sin(2t) + \theta_0)} dt \quad (4.11)$$

$$r(s) = r \quad (4.12)$$

Due to the complexity of the above integral, Equation (4.11) is solved nu-

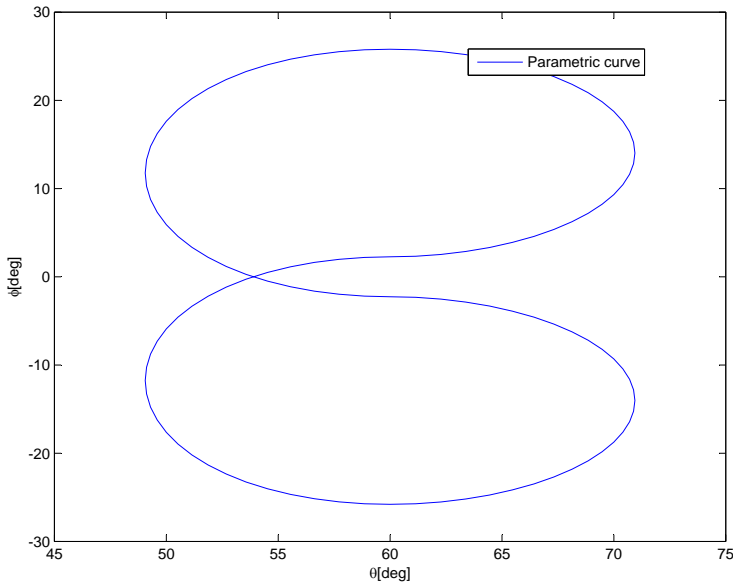


Figure 4.1: Parametric curve γ in $\theta\phi$ -plane.

merically. For the simulations a look-up table with interpolation in $\phi(s)$ is used.

In the propagation of s in equation (3.18), the angular velocity ω_{ep}^p is needed. Based on the curve $\gamma(s)$, the following method may be used to calculate ω_{ep}^p ,

[5]:

$$R_e^p = R_z(\beta_p)R_y(\theta_p)R_z(\phi_p) \quad (4.13)$$

$$\omega_{ep}^p = \omega_z(\dot{\beta}_p) + R_z(\beta_p)\omega_y(\dot{\theta}_p) + R_z(\beta_p)R_y(\theta_p)\omega_z(\dot{\phi}_p) \quad (4.14)$$

$$= \omega_{ep/s}^p \dot{s} \quad (4.15)$$

$$= \left(\omega_z\left(\frac{\partial\beta_p}{\partial s}\right) + R_z(\beta_p)\omega_y\left(\frac{\partial\theta_p}{\partial s}\right) + R_z(\beta_p)R_y(\theta_p)\omega_z\left(\frac{\partial\phi_p}{\partial s}\right) \right) \dot{s} \quad (4.16)$$

where $\frac{\partial\beta_p}{\partial s}$ is given:

$$\frac{\partial\beta_p}{\partial s} = \frac{\partial}{\partial s} \arctan \left(\frac{|\sin(4\pi\frac{s}{s_t})| \operatorname{sgn} \left(\sin(2\pi\frac{s}{s_t}) \right)}{\cos \left(4\pi\frac{s}{s_t} \right)} \right) \quad (4.17)$$

$$= \frac{4\pi}{s_t} \operatorname{sgn} \left(\cos(2\pi\frac{s}{s_t}) \right) \quad (4.18)$$

Due to the discontinuity in $\frac{\partial\beta_p}{\partial s}$, the following simplification is made in the controller from Equation (3.79). As mentioned previously, the term $\dot{\alpha}_1$ contains some terms that are difficult to implement.

$$\dot{\alpha}_1 = \frac{\partial}{\partial t} \left(-g_1(\mathbf{z}_1)^T \mathbf{z}_1 + \dot{\beta}_{h,d} - Kz_2 \right) \quad (4.19)$$

The terms $\frac{\partial}{\partial t} \left(g_1(\mathbf{z}_1)^T \mathbf{z}_1 + \dot{\beta}_{h,d} \right)$ are not implemented for the following simulations.

Recall from the equation for propagating the origin of the path frame along the curve, where the 4×4 -matrix was proven invertible in equation (3.19):

$$\begin{pmatrix} \dot{s} \\ \dot{y} \\ \dot{z} \\ \dot{x} \end{pmatrix} = \begin{pmatrix} 1 - \omega_{ep/s3}^p y + \omega_{ep/s2}^p z & 0 & 0 & 1 \\ \omega_{ep/s3}^p x - \omega_{ep/s1}^p z & 1 & 0 & 0 \\ -\omega_{ep/s2}^p x + \omega_{ep/s1}^p y & 0 & 1 & 0 \\ -\omega_{ep/s3}^p y + \omega_{ep/s2}^p z & 0 & 0 & 1 \end{pmatrix}^{-1} \begin{pmatrix} v_b^p \\ -k_x x \end{pmatrix} \quad (3.18)$$

4.3 Simulation with ideal conditions

The parameters used in these simulations are listed in Table 4.1, and the profile of the lift and drag coefficients is shown in Figure 2.5. The initial

Model parameter	value
<i>Kite:</i>	
m : Effective mass	10
A : Horizontal wing area	20
<i>Drag force:</i>	
C_{dm} : Minimum drag	0.05
k_d : Drag constant	0.05
<i>Lift force:</i>	
$C_{L,max}$: Maximum lift	1.5
c_{ls} : Lift slope	$1.5 \frac{\pi}{C_{L,max}}$
α_0 : De-power angle	$5 \frac{\pi}{180}$
<i>Crosswind force:</i>	
c_{cs} : Crosswind constant	1.1π
<i>Yawing moment:</i>	
c_{ks} : Directional stability	0.5
$c_{k,\delta,c}$: Effect of control input	1

Table 4.1: Model parameters

position is set:

$$x_{init} = \begin{pmatrix} \theta \\ \phi \\ \beta_b \\ \dot{\theta} \\ \dot{\phi} \\ \dot{\beta}_b \\ \delta_l \end{pmatrix} = \begin{pmatrix} 85^\circ \\ -50^\circ \\ -30^\circ \\ -5^\circ/s \\ 0 \\ 0 \\ 0 \end{pmatrix} \quad (4.20)$$

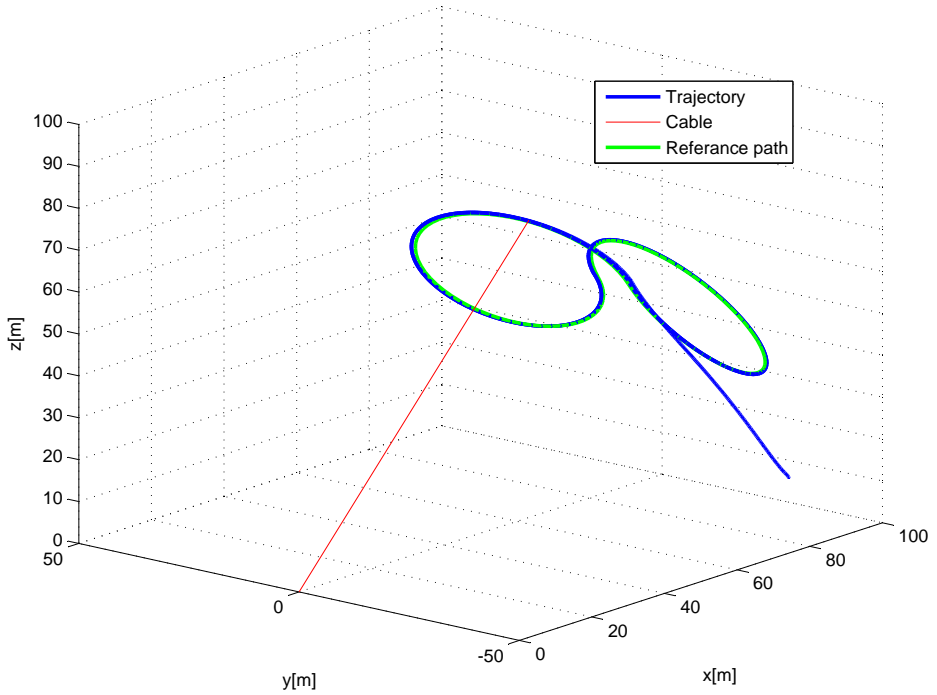


Figure 4.2: 3D-trajectory for the path-following system.

The wind is free of noise, $w = 10m/s$, and the path frame is initiated in $s = 0$:

$$\gamma(0) = \begin{pmatrix} 60^\circ \\ -25.8^\circ \\ r \end{pmatrix} \quad (4.21)$$

with the total length of the closed path $s_t = 240m$.

Figures 4.2-4.4 illustrates the trajectory of a 10 second simulation with ideal conditions. The kite converges to the reference path smoothly. As seen in

Figure 4.5, after convergence, there is some small ripple. This is due to the two left out terms in the controller.

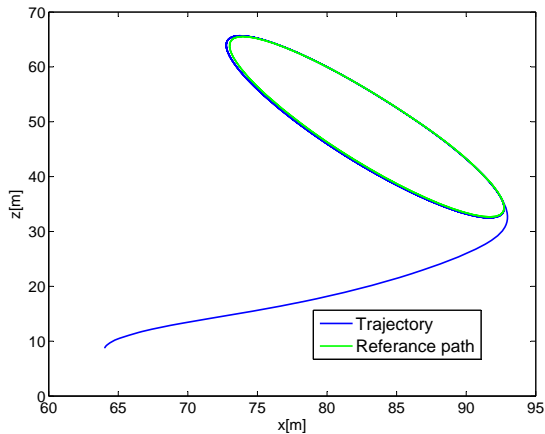


Figure 4.3: XZ-trajectory for the path-following system.

The desired yawing angle $\beta_{b,d}$ and the actual yawing angle is illustrated in Figure 4.6. β_b follows the desired value closely. The control input and the flaps angle seen in Figures 4.7 - 4.8 are fairly smooth. The oscillations occur in the interconnection between the two circular parts of the curve.

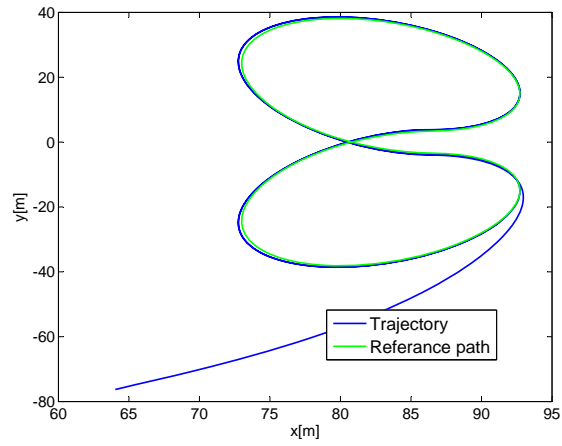


Figure 4.4: XY-trajectory for the path-following system.

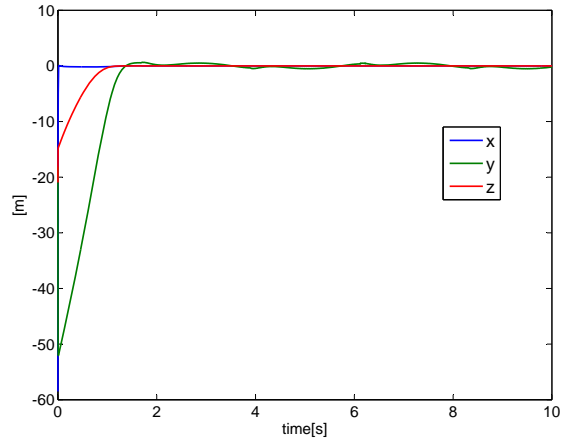


Figure 4.5: XYZ path error.

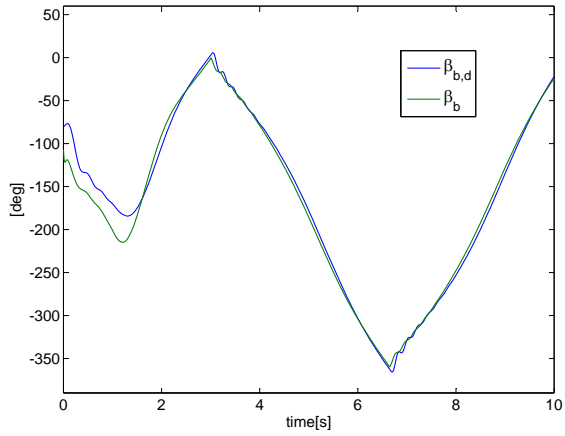
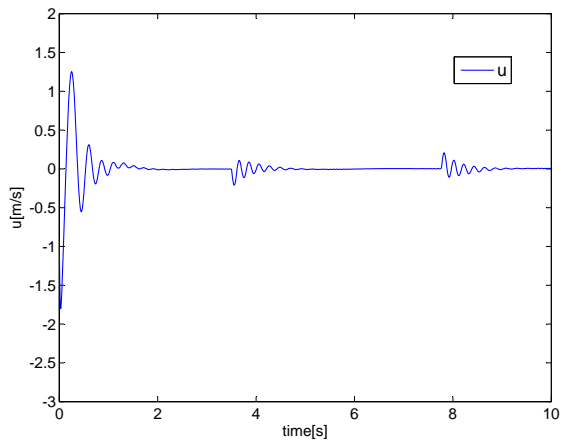
Figure 4.6: Yawing angles, β_b and $\beta_{b,d}$.

Figure 4.7: Control input from simulation.

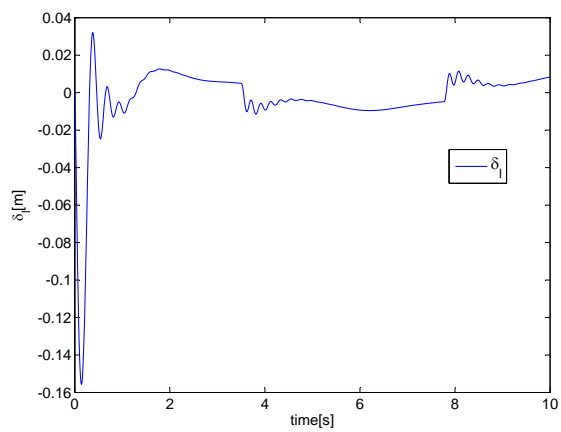


Figure 4.8: Control state δ_l .

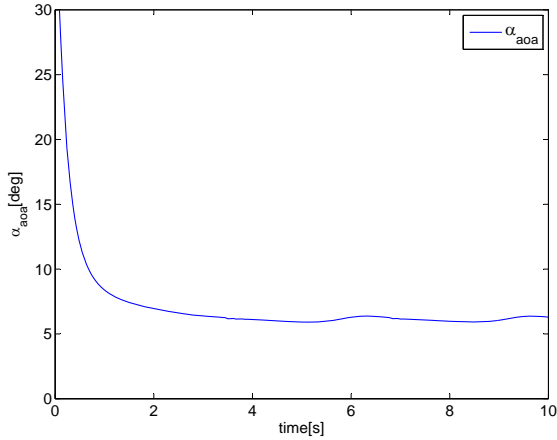


Figure 4.9: Angle of attack, α_{aoa} .

As stated in Chapter 2, for the approximations of the aerodynamic coefficients to be valid, the angle of attack is assumed to be small. Seen in Figure 4.9, α_{aoa} stabilizes around 7° . This is well within reasonable limits for the approximation, [10].

4.4 Simulation with wind turbulence

The initial position is set equal as in the case with ideal conditions. The wind vector is modelled as lowpass-filtered noise in both amplitude and direction. Nominal wind speed w is set to: $w = 6m/s$. Other parameters are kept the same as in the ideal case.

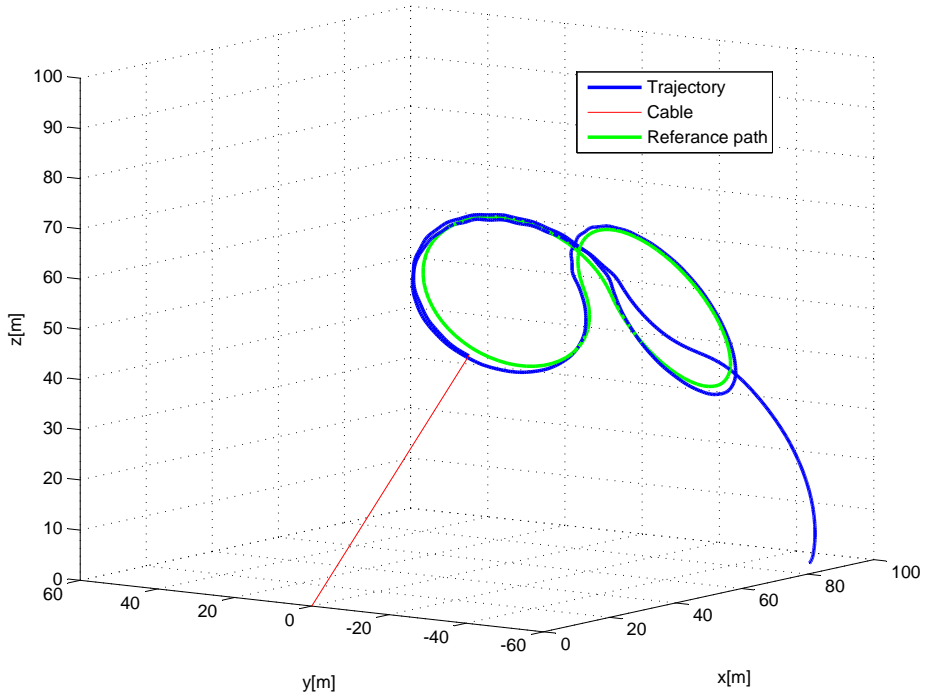


Figure 4.10: 3D-trajectory for the path-following system.

In Figures 4.10-4.12 the trajectory of a 10 second simulation with wind turbulence is plotted. As expected, some error is apparent. The response is similar to the case with no turbulence.

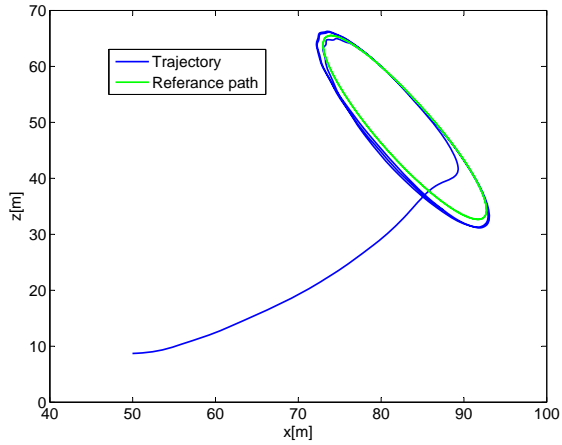


Figure 4.11: XZ-trajectory for the path-following system.

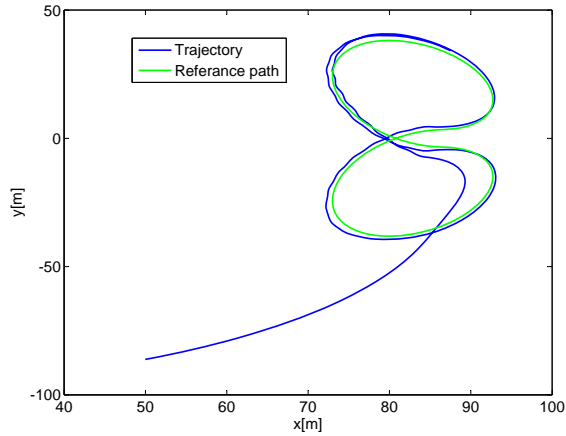


Figure 4.12: XY-trajectory for the path-following system.

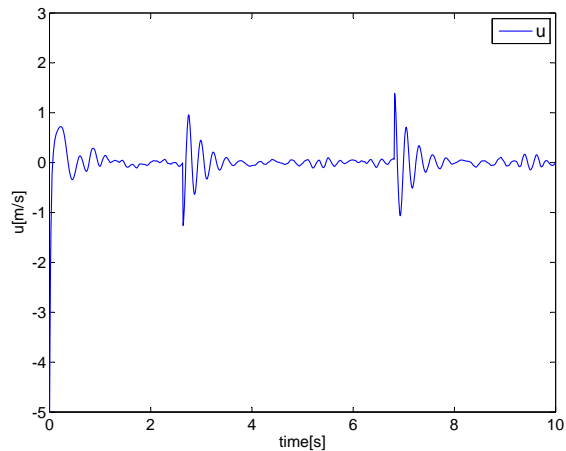
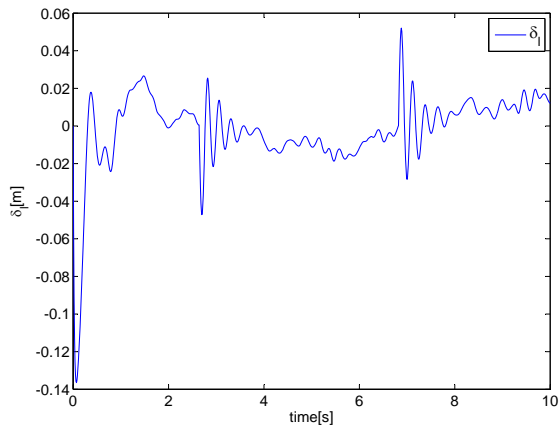
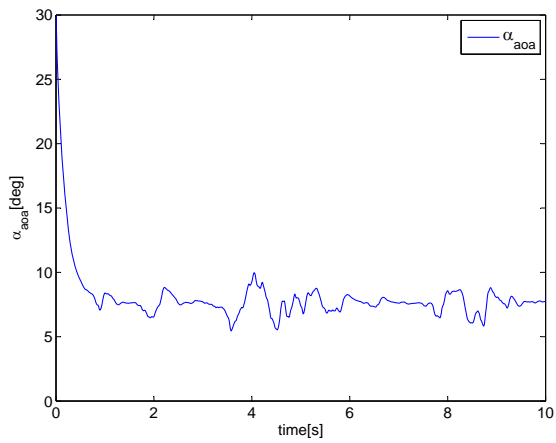


Figure 4.13: Control input from simulation.

The control input u and the flaps angle seen in Figure 4.13 and 4.14 are considerably more noisy in the case with wind turbulence.

Figure 4.14: Control state δ_l .Figure 4.15: Angle of attack, α_{aoa} .

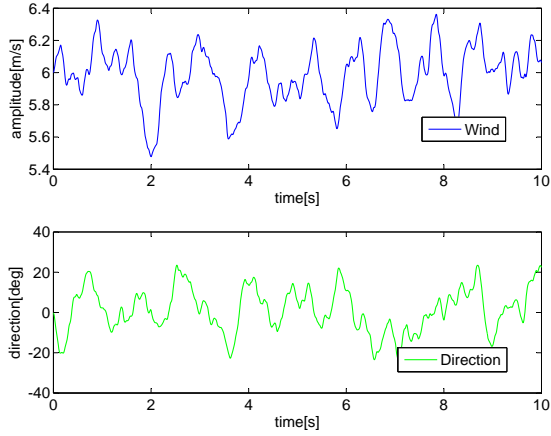


Figure 4.16: Wind speed and direction in the xy-plane.

The wind speed and direction for the case with turbulence is presented in Figure 4.16. The direction is given as the angle between the x-axis and the wind vector in the xy-plane of the earth frame \mathcal{F}_e .

Although the control system could not be proven stable for uncertainty in model parameters and wind, the simulation result indicate some robustness in the control system.

Chapter 5

Conclusion

In Chapter 2, a recognised model for tethered airfoils has been extended to include dynamics for the orientation of the body-frame. This orientation, the yawing angle in particular, is an important factor in understanding the dynamics of the system, and play an important role in the control system development. Although the model has not been compared to data from a real tethered airfoil, the simulations show realistic behaviour. This conclusion is drawn based on the authors experience with human-controlled kites as well as comparison to simulations of similar models presented by [9],[6].

The proposed controller in Chapter 3 asymptotically stabilizes the body-frame to a general path \mathcal{P} , locally in the set Ω_c . The set Ω_c includes the entire area of operation limited by the ground and the direction of the wind. Path-following is concluded to be a well suited control strategy for a tethered airfoil. To the author's best knowledge, the results presented in this thesis is the first to conclude on stability in a path-following system for tethered airfoils.

There are two parts of the control system: The line-of-sight inspired guidance system, and the lower level controller, following the guidance law. The guidance system is proven locally asymptotically stable, and is well suited

for any system where path-following control with use of spherical coordinates is desired.

Several studies [9] has been conducted on optimising trajectories for, and the use of MPC in control of tethered airfoils. In MPC, feedback control is needed to cope with model uncertainty [12]. The controller in Chapter 3 may serve as such a feedback controller.

Chapter 6

Further work

Path following control

The control system developed in this thesis, consists of a general guidance controller and a backstepping controller to follow this. The guidance law is applicable to any path-following system described in spherical coordinates, or moving along a spherical surface. The guidance controller is not proven Globally Asymptotically Stable on the described sphere. Although this is not necessary for the kite-system, it may be desirable for other applications.

Smooth control

The controller developed in chapter 3, Equation (3.79) is designed to cancel out any perturbing terms. It contains variables that may be noisy, or be difficult to implement. Such a controller would result in more rapid wear and tear in actuators and other hardware.

State - and Parameter estimation For control systems that are based on a kinematic model, including the one discussed in Chapter 3, parameter estimation is an important issue, as the stability analysis may rely on the model parameters. This should be addressed in relation to a robustness analysis. State estimation is an obvious topic for further work, because in any closed loop system needs state measurements or estimates to calculate

the control input.

Robustness

The assumptions made in Chapter 3, state that full state measurements and exact model insight is available. This is not the case for real systems, where model errors and vague wind estimates are likely to occur. A robustness analysis should be performed with the control system in order to conclude on noise rejection and sensitivity to model errors.

Prototype testing

Last, but not least, one should test the control system in a real application.

Bibliography

- [1] Kitegen. <http://kitegen.com/>. Accessed: 02/06/2011.
- [2] World sailing speed record council. <http://www.sailspeedrecords.com/>. Accessed: 02/06/2011.
- [3] Even Børhaug. Cross-track maneuvering and way-point control of underactuated auvs in particular, and mechanical systems in general. 2005.
- [4] Mermout Burger. Disturbance rejection using conditional integrators. Master's thesis, NTNU, 2011.
- [5] Olav Egeland and Jan Tommy Gravdahl. *Modeling and Simulation for Automated Control*. 2002.
- [6] Lorenzo Fagiano. Control of tethered airfoils for high-altitude wind energy generation. 2009.
- [7] Weir Hass and Thomas. *University Calculus*. 2007.
- [8] Boris Houska. Robustness and stability optimization of open-loop controlled power generating kites. 2007.
- [9] Andreas Ilzhoefer. *Real-time Automatic Control and Estimation with Application to Power Generating Kites under Varying Wind Conditions*. PhD thesis, 2007.

- [10] Jr. John D. Anderson. *Fundamentals of Aerodynamics*. Fourth edition, 2005.
- [11] Håvard Knappskog. Automated control of kites for electricity generation. Master's thesis, NTNU, 2010.
- [12] Jan Marian Maciejowski. *Predictive Control with Constraints*. 2002.
- [13] W. Mark Spong, Seth Hutchinson, and M. Vidyasagar. *Robot Modelling and Control*. 2006.
- [14] Brian L. Stevens and Frank L. Lewis. *Aircraft Control and Simulation*. Second edition, 2003.